Fraunhofer Institut
Techno- und
Wirtschaftsmathematik

C. Lautensack, A. Särkkä, J. Freitag, K. Schladitz

Anisotropy analysis of pressed point processes

Berichte des Fraunhofer ITWM, Nr. 141 (2008)

ISSN 1434-9973

Bericht 141 (2008)

Die Veröffentlichungen in der Berichtsreihe des Fraunhofer ITWM können bezogen werden über:

Fraunhofer-Institut für Techno- und
Wirtschaftsmathematik ITWM
Fraunhofer-Platz 1

67663 Kaiserslautern
Germany

Telefon: 06 31/3 16 00-0
Telefax: 06 31/3 16 00-10 99
E-Mail: info@itwm.fraunhofer.de
Internet: www.itwm.fraunhofer.de

Vorwort

Das Tätigkeitsfeld des Fraunhofer-Instituts für Techno- und Wirtschaftsmathematik ITWM umfasst anwendungsnahe Grundlagenforschung, angewandte Forschung sowie Beratung und kundenspezifische Lösungen auf allen Gebieten, die für Techno- und Wirtschaftsmathematik bedeutsam sind.

In der Reihe »Berichte des Fraunhofer ITWM« soll die Arbeit des Instituts kontinuierlich einer interessierten Öffentlichkeit in Industrie, Wirtschaft und Wissenschaft vorgestellt werden. Durch die enge Verzahnung mit dem Fachbereich Mathematik der Universität Kaiserslautern sowie durch zahlreiche Kooperationen mit internationalen Institutionen und Hochschulen in den Bereichen Ausbildung und Forschung ist ein großes Potenzial für Forschungsberichte vorhanden. In die Berichtreihe sollen sowohl hervorragende Diplom- und Projektarbeiten und Dissertationen als auch Forschungsberichte der Institutsmitarbeiter und Institutsgäste zu aktuellen Fragen der Techno- und Wirtschaftsmathematik aufgenommen werden.

Darüber hinaus bietet die Reihe ein Forum für die Berichterstattung über die zahlreichen Kooperationsprojekte des Instituts mit Partnern aus Industrie und Wirtschaft.

Berichterstattung heißt hier Dokumentation des Transfers aktueller Ergebnisse aus mathematischer Forschungs- und Entwicklungsarbeit in industrielle Anwendungen und Softwareprodukte – und umgekehrt, denn Probleme der Praxis generieren neue interessante mathematische Fragestellungen.

Prof. Dr. Dieter Prätzel-Wolters
Institutsleiter

Kaiserslautern, im Juni 2001

Anisotropy analysis of pressed point processes

Claudia Lautensack*
University of Applied Sciences, Darmstadt
Fraunhofer Institute for Industrial Mathematics (ITWM), Kaiserslautern

Aila Särkkä
Department of Mathematical Sciences, Chalmers University of Technology, Göteborg

Johannes Freitag
Alfred Wegener Institute for Polar and Marine Research, Bremerhaven

Katja Schladitz
Fraunhofer Institute for Industrial Mathematics (ITWM), Kaiserslautern

Abstract

This paper introduces methods for the detection of anisotropies which are caused by compression of regular three-dimensional point patterns. Isotropy tests based on directional summary statistics and estimators for the compression factor are developed. These allow not only for the detection of anisotropies but also for the estimation of their strength. Using simulated data the power of the methods and the dependence of the power on the intensity, the degree of regularity, and the compression strength are studied. The motivation of this paper is the investigation of anisotropies in the structure of polar ice. Therefore, our methods are applied to the point patterns of centres of air pores extracted from tomographic images of ice cores. This way the presence of anisotropies in the ice caused by the compression of the ice sheet as well as an increase of their strength with increasing depth are shown.

Keywords: estimation of compression, isotropy test, nearest neighbour distance, orientation analysis, polar ice, Ripley's K function

*claudia.lautensack@itwm.fraunhofer.de

1 Introduction

Polar ice is a remarkable multi-proxy archive for climate information of the past. With the perspective of highly resolved time series over hundreds of thousand years it has attracted considerable interest of climate researchers. During the last decades a couple of deep polar ice cores were drilled through the Antarctic and Greenlandic ice sheets. Several proxy parameters are identified in the ice, e.g. temperature, precipitation, dust, aerosol, sea ice extent, biological activity, and atmospheric composition including the famous records of trace and greenhouse gases (Bender et al. (1994), EPICA community members (2004), EPICA community members (2006)). Accurate chronologies are an important requirement for the interpretation of ice core records. However they are not satisfyingly developed until now. No absolute dating tool is available for polar ice. The recent dating relies on models. A key element of them are the simulations of the individual history of ice deformation for each specific core site. In this paper we present the first direct method for the estimation of the deformation history (expressed by the thinning function as explained below) in polar ice using the measured anisotropy of air inclusions in centimetre sized ice samples from a deep ice core.

An idealised ice sheet consists of a vertical sequence of compressed snow layers that have been buried under the load of newly fallen snow. Because ice under pressure is subject to creep there is a vertical compression accompanied by a total lateral transport of ice from the interior of an ice sheet to its boundaries. At the boundaries the ice is exported to the ocean via iceberg calving and melting. Due to the interaction of compression and lateral transport, the pore structures at different compression rates do not differ significantly at first sight. In particular, counterintuitively the number of pores per volume does not increase considerably owing to the incompressibility of the ice. Furthermore, even ice samples taken from the same depth show a high variability in their pore structure by reason of seasonal variations and the small sample size. CT imaging can only handle centimetre sized samples while the compression rates vary on scales of 10 metres. The key question is therefore, whether the compression rate can be deduced from the pore structure.

The age of an ice layer is defined as the time when the water molecules of such a layer have been accumulated on the surface of the ice sheet as snow. At undisturbed sites the age is continuously increasing with depth with the oldest ice at the bottom. The oldest ice drilled so far is dated back to about 100 000 years in Greenland (Summit station, 72°34′ N, 37°37′ W, GRIP ice core) and to about 800 000 years in Antarctica (Dome Concordia station, 75°06′ S, 123°20′ E, EPICA-EDC ice core). Flow models that are used for dating describe the thinning of annual layers with depth based on a mechanical model and on assumptions about bedrock conditions and surface elevation changes in the past (Paterson (1994),

Parrenin et al. (2007), 2007, Ruth et al. (2007), Severi et al. (2007)). Then the derived thinning function is combined with a snow accumulation model for the past to estimate the age of the ice as a function of depth. Diverse input parameters of such models are not well constrained including the mechanical properties of polycrystalline ice with different chemical load and crystal orientation (a topic of growing interest which is not fully understood, Duval (2000)) with consequences for the formulation of the constitutive law in the mechanical model. Due to the complex interaction between bedrock and ice it will also be difficult to formulate a physical model for the flow conditions at the bedrock boundary. Parrenin et al. (2007) tried to avoid these problems in the model parametrisations by the application of an inverse method using some fixed absolute age markers in the core.

In this paper we show that the total thinning in polar ice could be directly retrieved from measured air inclusions in combination with a statistical method analysing pressed point processes. We have chosen unmarked summary statistics because the anisotropy cannot be seen in the shape of the pores, which are more or less spherical on the deeper layers. In our first attempt the application is restricted to samples from an ice core drilled at a Dome position where the acting forces are known. In the case of a Dome one can assume that ice deforms simply in uni-axial compression. Ice layers are compressed by a factor of c in the vertical and stretched in the lateral direction by a factor of $1/\sqrt{c}$ keeping the total volume constant. The factor c gives the total thinning of an ice layer. The bubble-like air inclusions inside the ice matrix are used as strain markers. They are relicts of a long-term sintering process in the firn column. The term firn refers to the upper 50 to 100 m of an ice sheet and describes sintered ice grains with connected air-filled pores in between. The ice grains form an ensemble of tetrakaidecahedrons with the air located at their edges. At the firn-ice transition the interconnected pore space starts to isolate in individual bubbles. Firn becomes ice per definition. During the sintering and compaction the pore volume is continuously decreasing from 50% to about 10% of the total volume at the firn-ice transition. The close-off process results in a quite regular and uniform distribution of bubbles within the ice. Their regularity originates from the initial homogeneity of surface snow and the moderate sintering conditions, particularly the long sintering time with only slowly increasing pressure load. The mean distance between adjacent bubbles is of the order of the grain size and this is about 1 mm at the firn-ice transition. Below the firn-ice transition the bubble distributions are only affected by the overall deformation process of the ice itself. Bubble migration due to further grain growth or small temperature gradients is negligible. The increasing pressure with depth leads to bubble shrinkage but again without affecting the distribution of the bubble centres. At pressure loads below about 600 to 700 m depth the bubbles become unstable and the enclosed air is captured as clathrates in the

ice. There is a natural depth limit for the existence of bubbles in polar ice and therefore for the application of our method to deep polar ice cores.

The paper is organised as follows. First, we introduce some directional summary statistics in 3D, which are then used as the basis for some isotropy tests. The tests are constructed in order to reveal the particular type of anisotropy caused by simultaneous compression and lateral transport. In Section 4 we perform a simulation study comparing the powers of the tests based on different summary statistics. The estimation of the pressing factor is discussed in Section 5. Both studies are performed on a more general level than needed for the analysis of the ice samples in order to explore the range of applicability of the suggested methods. Finally, the methods are applied to the air pore data. The anisotropy of air pores is studied and the pressing factors are estimated at different depths.

2 Directional summary statistics

There are several summary statistics which can be used to study the spatial distribution of a point pattern. The nearest neighbour distance distribution function G is the distribution function of the distance from a typical point of the process to its nearest neighbour. The empty space function F is the distribution of distance to the nearest point of the process from a random point in space. The J function is a combination of the G and the F function. Finally, Ripley's K function is related to the expected number of further points of the process within a certain distance from a typical point of the point process and the pair-correlation function g is essentially the derivative of the K function w.r.t. the distance (for all these functions, see e.g. Diggle (2003)). Originally, these functions have been defined in 2D but they can be defined exactly in the same way for three-dimensional point processes. Usually, these statistics assume that the point pattern is a realisation of a stationary and isotropic point process.

Here, we are interested in detecting possible anisotropies which requires directional counterparts of these functions. So far, this problem has only been studied in the 2D case. Stoyan and Beneš (1991) discuss different types of anisotropies in marked point patterns, namely anisotropies of marks (orientation of marks) and anisotropic distribution of points. They define the point-pair-rose-density, which describes the anisotropy of the arrangement of points, possibly including information on the marks. The idea is as follows. Choose a pair of points with distance in a certain interval (r_1, r_2) at random, and determine the angle β between the line going through the points and the 0-direction. This angle is a random variable taking values between 0 and π, whose distribution gives information on the arrangement of the points. The point-pair rose density $o_{r_1 r_2}(\beta)$ is the corresponding probability density function (weighted by the marks). It is an

integrated version of the anisotropic pair-correlation function which is defined as follows (Stoyan, 1991). The second-order product density $\varrho(x_1, x_2)$ is related to the probability of finding points of the process in small neighbourhoods of both x_1 and x_2. In the stationary but anisotropic case, ϱ is a function of the distance r and the angle φ between the line going through x_1 and x_2 and the 0-direction. The anisotropic pair correlation function is then $g(r, \varphi) = \varrho(r, \varphi)/\lambda^2$, where λ is the intensity of the point process. Both for the point-pair rose density and the anisotropic pair-correlation function an edge-corrected kernel estimator should be used. Furthermore, Stoyan et al. (1995, p.127) define a directional version of Ripley's K function.

The definitions of these functions carry over to the 3D case without any difficulties. However, the practical evaluation as well as the visualisation of the results becomes more challenging. Already in 2D, directional summary statistics depend on two variables, the distance and the angle. Nevertheless, it is obvious how to divide a disc into sectors of equal size such that the summary statistics can be estimated for a discrete set of parameters. Circular diagrams or plots over the interval $[0, 2\pi]$ can then be used to display the results.

In 3D, three variables, the distance and two angles, have to be used. The estimation of the directional summary statistics with respect to different directions requires a suitable partition of the ball. The sectors should be of equal size and shape, which means that the directions should be distributed as uniformly as possible. Other choices might hold the danger of introducing some structure in the results which is caused by the partitioning of the ball rather than by the data. In general, it is not clear how to choose such a partition in a way that it is easily parametrised e.g. by means of spherical coordinates.

Here, we are dealing with a special type of anisotropy, namely anisotropy in z-direction caused by compression of the point process. In this case, the behaviour of the point process in z-direction has to be compared to other reference directions, e.g. the x- and y-direction. For this purpose, the process has to be studied within suitable sets aligned along these directions. A complete partitioning of the ball is not necessarily required.

One type of ball segments which are described easily in spherical coordinates, and therefore suitable for our application, are spherical cones. Let $C_u(r, \theta)$ with $r \geq 0$ and $0 \leq \theta \leq \pi$ denote a double spherical cone defined as

$$C_u(r, \theta) = \left\{ R_u \begin{pmatrix} s \sin\vartheta \cos\varphi \\ s \sin\vartheta \sin\varphi \\ s \cos\vartheta \end{pmatrix} : s \in [0, r], \vartheta \in [0, \theta] \cap [\pi - \theta, \pi], \varphi \in [0, 2\pi] \right\},$$

where u is a unit vector and R_u is a rotation mapping the z-axis on the line spanned by u. In order to detect anisotropies, the point pattern is observed within three double cones aligned along the coordinate axes and centred in the

typical point of the process. A compressed point process will have a different appearance within the z-cone than within the x- and y-cones.

In the following we define the directional summary statistics which will be used to detect the anisotropies. Already Stoyan et al. (1995, p.153) discuss how to use the directional K function and its zero-contours to estimate the pressing factor of pressed point patterns. Therefore, the directional K function is the first function to be considered here. The density functions mentioned above, namely the point-pair rose density and the anisotropic pair-correlation function, are good when investigating and describing anisotropies in a particular point pattern. However, these functions are usually estimated by using kernel estimators. In addition to the technical problems in 3D, an analysis based on these functions would therefore pose further questions such as the choice of a suitable bandwidth. For testing and estimation purposes it might be a better idea to use cumulative functions like the directional K function. Smaller local fluctuations in the cumulative functions should make the comparison of the results for different directions more stable. In addition to the directional K function, we will therefore consider two directional counterparts of the nearest neighbour distance distribution function G.

2.1 Directional K function K_{dir}

We consider a directional version of Ripley's K-function, namely the second reduced moment measure of the cone $C_u(r,\theta)$ which is denoted by $K_{\mathrm{dir},u,\theta}(r)$. This means that $K_{\mathrm{dir},u,\theta}(r)$ is the expected number of points within the double cone centred in a typical point of the point process Ψ. An unbiased estimator of $\lambda^2 K_{\mathrm{dir},u}(r)$ is given by

$$\lambda^2 \hat{K}_{\mathrm{dir},u,\theta}(r) = \sum_{x\in\Psi} \sum_{y\in\Psi, y\neq x} \frac{\mathbb{1}_{C_u(r,\theta)}(x-y)}{|W_x \cap W_y|},\ r \geq 0, \tag{1}$$

where W_x is the translation of the window W by the vector x and $|B|$ denotes the volume of a set $B \subset \mathbb{R}^3$ (Stoyan et al., 1995, p. 134 f).

2.2 Directional G functions

Pressing a hard core point pattern will transform the empty ball centred in each point of the process into an ellipsoid. Therefore, this particular kind of anisotropy will influence the distribution of the distance to the nearest neighbour. The nearest neighbour in z-direction will be closer than the nearest neighbour in x- or y-direction. Depending on whether the nearest neighbour is determined locally or globally, this gives rise to the following summary statistics:

2.2.1 Local G function G_{loc}

Here, the nearest neighbour is defined locally, i.e. we are looking for the nearest neighbour contained in the cone $x + C_u(r, \theta)$ centred in a point $x \in \Psi$. Denote by $G_{\mathrm{loc},u,\theta}$ the distribution function of the distance from the typical point of the process to the closest point in the cone. In order to define an estimator for $G_{\mathrm{loc},u,\theta}$, mark each point $x \in \Psi$ with the distance d to the closest point in $x + C_u(r, \theta)$ and consider the distribution of the distance d. We use a Hanisch type estimator for $G_{\mathrm{loc},u,\theta}$ given by

$$\hat{G}_{\mathrm{loc},u,\theta}(r) = \frac{\hat{G}_{H,\mathrm{loc},u,\theta}(r)}{\hat{\lambda}_H} \tag{2}$$

with

$$\hat{G}_{H,\mathrm{loc},u,\theta}(r) = \sum_{(x,d)\in\Psi} \frac{\mathbb{1}_{[0,r]}(d)\, \mathbb{1}_{W\ominus C_u(d,\theta)}(x)}{|W \ominus C_u(d,\theta)|},\ r \geq 0,$$

and

$$\hat{\lambda}_H = \sum_{(x,d)\in\Psi} \frac{\mathbb{1}_{W\ominus C_u(d,\theta)}(x)}{|W \ominus C_u(d,\theta)|}.$$

The term $W \ominus C_u(d, \theta)$ denotes the erosion of the window W by the cone $C_u(d, \theta)$ and is included for edge correction. We consider only those points $x \in \Psi$ with the property that the complete cone $x + C_u(d, \theta)$ is contained in the observation window W. As in Hanisch (1984) it can be shown that $\hat{G}_{H,\mathrm{loc},u,\theta}$ is an unbiased estimator for $\lambda G_{\mathrm{loc},u,\theta}$.

2.2.2 Global G function G_{glob}

In this case we determine the global nearest neighbour $y \in \Psi$ for each point $x \in \Psi$. Then, $G_{\mathrm{glob},u,\theta}$ is defined as the distribution function of the distance between x and y conditioned on $y \in x + C_u(r, \theta)$. An estimator for $G_{\mathrm{glob},u,\theta}(r, \theta)$ is then given by

$$\hat{G}_{\mathrm{glob},u,\theta}(r) = \frac{\sum\limits_{(x,y)\in\Psi} \mathbb{1}_{C_u(r,\theta)}(x-y)\, \mathbb{1}_{W\ominus b(0,||x-y||)}(x)}{\sum\limits_{(x,y)\in\Psi} \mathbb{1}_{C_u(\infty,\theta)}(x-y)\, \mathbb{1}_{W\ominus b(0,||x-y||)}(x)},\ r \geq 0. \tag{3}$$

Here, we consider only the points $x \in \Psi$ with the property that the ball $b(x, ||x - y||)$ is completely contained in W.

Compared to G_{loc}, the global G function depends on a smaller number of points of Ψ. Therefore, G_{loc} should yield better results for small intensities, while, being related to the nearest-neighbour orientation density, G_{glob} might be a good

alternative in the case of high intensity patterns. A drawback of the G functions might be their 'short-sightedness' which is caused by the consideration of only nearest neighbours (Illian et al., 2008, p.214). Even though the phenomena we are studying are rather local, the use of second order methods such as K_{dir} might be expected to yield better results.

3 Isotropy tests

In the following, we introduce some tests which seem suitable to detect anisotropies caused by pressing of isotropic hard core point processes. Monte Carlo tests are very common tests in spatial statistics (Stoyan and Stoyan, 1994). This technique, however, requires an appropriate model for the data under investigation. Deviations between the model and the data might then result in a loss of power of the related tests. Since we are working with replicated data, we will therefore concentrate on non-parametric methods which are only based on estimations from the data and do not require further simulations.

3.1 Tests using summary statistics

Let $\hat{S}_x$, $\hat{S}_y$, and $\hat{S}_z$ be estimators of one of the summary statistics introduced above with respect to the x-, y-, and z-direction. In the isotropic case, all three estimates will look similar. For the pressed pattern only $\hat{S}_x$ and $\hat{S}_y$ should be similar but show a clear deviation from $\hat{S}_z$.

Consider n point patterns $\psi_1, \ldots, \psi_n$ which can be assumed to have the same distribution and should be tested for isotropy. If the number of samples n is large, a test can be based on a comparison of the test statistics

$$T_{xy,i} = \int_{r_1}^{r_2} |\hat{S}_{x,i}(r) - \hat{S}_{y,i}(r)|\, dr, \quad i = 1, \ldots, n$$

and

$$T_{z,i} = \min\left(\int_{r_1}^{r_2} |\hat{S}_{x,i}(r) - \hat{S}_{z,i}(r)|\, dr, \int_{r_1}^{r_2} |\hat{S}_{y,i}(r) - \hat{S}_{z,i}(r)|\, dr \right), \quad i = 1, \ldots, n$$

where $[r_1, r_2]$ is a given interval. T_z is defined using the minimum to make sure that the z-direction differs from both the x- and the y-direction. Other choices such as the mean or the maximum could be considered as well. The isotropy hypothesis for a certain sample ψ_i is rejected at significance level α if the corresponding value $T_{z,i}$ is larger than $100(1-\alpha)\%$ of the estimated T_{xy} values.

If only a few samples are available, a Monte Carlo test using the test statistic

$$T_{\sum} = \int_{r_1}^{r_2} \left(|\hat{S}_x(r) - \hat{S}_y(r)| + |\hat{S}_y(r) - \hat{S}_z(r)| + |\hat{S}_z(r) - \hat{S}_x(r)| \right) dr,$$

can be considered alternatively. Then, the theoretical value of $T_{\sum}$ under an isotropic model is equal to 0. This test, however, requires the existence and the simulation of an appropriate model for the data.

The alternative statistics

$$T'_{xy} = \max_{r_1 \le r \le r_2} |\hat{S}_x(r) - \hat{S}_y(r)|,$$

$$T'_z = \min \left(\max_{r_1 \le r \le r_2} |\hat{S}_x(r) - \hat{S}_z(r)| \, , \max_{r_1 \le r \le r_2} |\hat{S}_y(r) - \hat{S}_z(r)| \right),$$

and

$$T'_{\sum} = \max_{r_1 \le r \le r_2} \left(|\hat{S}_x(r) - \hat{S}_y(r)| + |\hat{S}_y(r) - \hat{S}_z(r)| + |\hat{S}_z(r) - \hat{S}_x(r)| \right)$$

were also considered in first trials, but performed worse than the integral statistics above due to large local differences between the functions $\hat{S}_x$, $\hat{S}_y$, and $\hat{S}_z$.

3.2 Direction to the nearest neighbour

The compression of a hard core point process will result in a pattern where the points are closer in z-direction than they are in x- or y-direction. Therefore, the direction to the nearest neighbour after pressing will have a preferred direction along the z-axis. As an alternative to the tests using directional summary statistics, we test this directional distribution for uniformity against the alternative of a preferred direction using the test described in Anderson and Stephens (1972). This provides us with another model-free method, whose advantage is its simplicity. It only requires the computation of the directions to the nearest neighbours, a further choice of parameters such as the interval $[r_1, r_2]$ or the size of the cone is not necessary. However, looking only at directions, rather than directions and distances, this test might be less powerful than tests based on both quantities.

The uniformity test works as follows. Suppose a set of unit vectors $v_i = (x_i, y_i, z_i), i = 1, \ldots, n$, is given. Then compute the orientation matrix

$$A = \begin{pmatrix} \sum x_i^2 & \sum x_i y_i & \sum x_i z_i \\ \sum x_i y_i & \sum y_i^2 & \sum y_i z_i \\ \sum x_i z_i & \sum y_i z_i & \sum z_i^2 \end{pmatrix}.$$

Denote the eigenvalues of A by $\lambda_1 \geq \lambda_2 \geq \lambda_3$ and the corresponding eigenvectors by u_1, u_2, and u_3. The value of λ_1 is used as a test statistic for the uniformity test against a bimodal alternative. If λ_1 is too large, the uniformity hypothesis is rejected and u_1 yields a maximum likelihood estimate of the modal vector. For $n > 100$, the significance points for λ_1 at a 5% significance level are given by $\frac{1}{3} + \frac{0.873}{\sqrt{n}}$.

4 Simulations

In the following, we will evaluate the powers of the anisotropy tests introduced above applying them to simulated data. We believe that our methods could be applied to both clustered and regular point patterns. Nevertheless we restrict ourselves to hard core point processes since the air pore structures are regular. In order to cover a wide range of such patterns, we are going to study two established models: a Matérn hard core point process and a random packing of balls with a much higher degree of regularity. The choice of the parameter values in the simulations (intensity, hard core radius) is motivated by the values in the ice data. Isotropic realisations of both models are scaled by the vector $(\frac{1}{\sqrt{c}}, \frac{1}{\sqrt{c}}, c)$ with $0 < c \leq 1$. This means the patterns are compressed in z-direction but stretched in x- and y-direction such that the volume of the observation window is preserved. For the estimation of the summary statistics the value $\theta = \frac{\pi}{4}$ was chosen, which yields reasonably large but still non-overlapping cones.

4.1 Matérn hard core point process

Realisations of Matérn hard core point processes with intensities $\lambda = 500$ and hard core radius $R = 0.025, 0.05$, and 0.075 as well as $\lambda = 1000$ and $R = 0.025$ and 0.05 were simulated. The isotropic realisations were generated within the cuboids $[0, \sqrt{c}] \times [0, \sqrt{c}] \times [0, \frac{1}{c}]$ with $c = 0.7, 0.8$, and 0.9. The pressing of these realisations with the factor c then yielded point patterns within the unit cube. For each set of parameters, we simulated 1000 realisations of the pressed point patterns. Each of these realisations was tested for isotropy using the tests based on $G_{\text{loc}}, G_{\text{glob}}$, and K_{dir}. Good results of the estimation can only be expected if the envelopes of the directional summary statistics are disjoint on the chosen observation interval. For the largest hard core values considered in Figures 1 and 2, this is the case on the interval $[0, 1.1R]$ which was therefore chosen for the computation of the test statistics. In order to check the dependence of the test results on the choice of the interval, the alternatives $[0, \frac{4R}{3}]$ and $[0, 0.1]$ ($[0, 0.1]$ and $[0, 0.2]$ for $R = 0.075$) were also considered.

Furthermore, the uniformity test for the direction to the nearest neighbour

Table 1: Powers of the isotropy tests using directional summary statistics on a 5% significance level for 1000 Matérn hard core point patterns of intensity $\lambda = 500$ and hard core radius R pressed by the factor c. The test statistics were computed on the interval $[0, r_2]$.

c | R	0.025	0.025	0.025	0.05	0.05	0.05	0.075	0.075	0.075
0.9 | r_2	0.1	0.033	0.0275	0.1	0.067	0.055	0.2	0.1	0.0825
G_{loc}	**1.4**	6.6	26.6	3.7	23.2	77.9	18.0	65.7	98.9
G_{glob}	0.6	6.1	**26.8**	**4.8**	22.3	73.9	**39.1**	56.6	87.0
K_{dir}	1.0	**7.0**	26.7	4.5	**26.7**	**82.6**	7.9	**78.0**	**99.7**
0.8 | r_2	0.1	0.033	0.0275	0.1	0.067	0.055	0.2	0.1	0.0825
G_{loc}	**1.4**	21.9	49.3	15.4	72.7	97.2	77.8	99.8	**100**
G_{glob}	1.0	21.2	48.0	**21.3**	68.2	96.6	**93.9**	98.6	**100**
K_{dir}	1.3	**23.3**	**49.9**	19.9	**79.7**	**98.8**	36.9	**100**	**100**
0.7 | r_2	0.1	0.033	0.0275	0.1	0.067	0.055	0.2	0.1	0.0825
G_{loc}	**1.9**	**37.9**	56.3	41.4	95.0	99.3	98.3	**100**	**100**
G_{glob}	**1.9**	36.1	56.2	**50.7**	91.6	98.1	**98.9**	99.7	**100**
K_{dir}	1.6	**37.9**	**57.7**	44.6	**98.1**	**99.6**	75.7	**100**	**100**

was applied. The powers of the tests for $\lambda = 500$ are given in Table 1, the results for $\lambda = 1000$ are displayed in Table 2. The results for the test based on the eigenvalue λ_1 are shown in Table 3.

As expected, higher powers are achieved for higher intensities, larger hard core radii and stronger pressing. In all cases, the best results were obtained on the interval $[0, 1.1R]$. Comparing the powers for different summary statistics on this interval, we see that K_{dir} usually yields the best results. Only for $R = 0.025$ and $c = 0.9$, i.e. for the smallest hard core radius and the weakest pressing considered, it is one of the G functions which performs slightly better. Also, both G functions, especially G_{glob}, turn out to be more robust when changing the interval of observation. This can be explained by the fact that both functions are distribution functions which stabilize at a value of 1 for large values of r. The conjecture that tests based on summary statistics are superior to the test based on the eigenvalues of the orientation matrix is confirmed if the integration intervals for the summary statistics are chosen suitably.

The mean numbers of points contributing to the estimation of the G functions for the point patterns of intensity 500 are shown in Table 4. As expected, the numbers are much smaller for G_{glob} than for G_{loc}. When increasing the pressing factor, a decrease of the numbers for the x- and y-direction is observed while the numbers for the z-direction increase. This tendency is more pronounced for G_{glob} than for G_{loc}. In extreme cases it might lead to instabilities in the estimation of

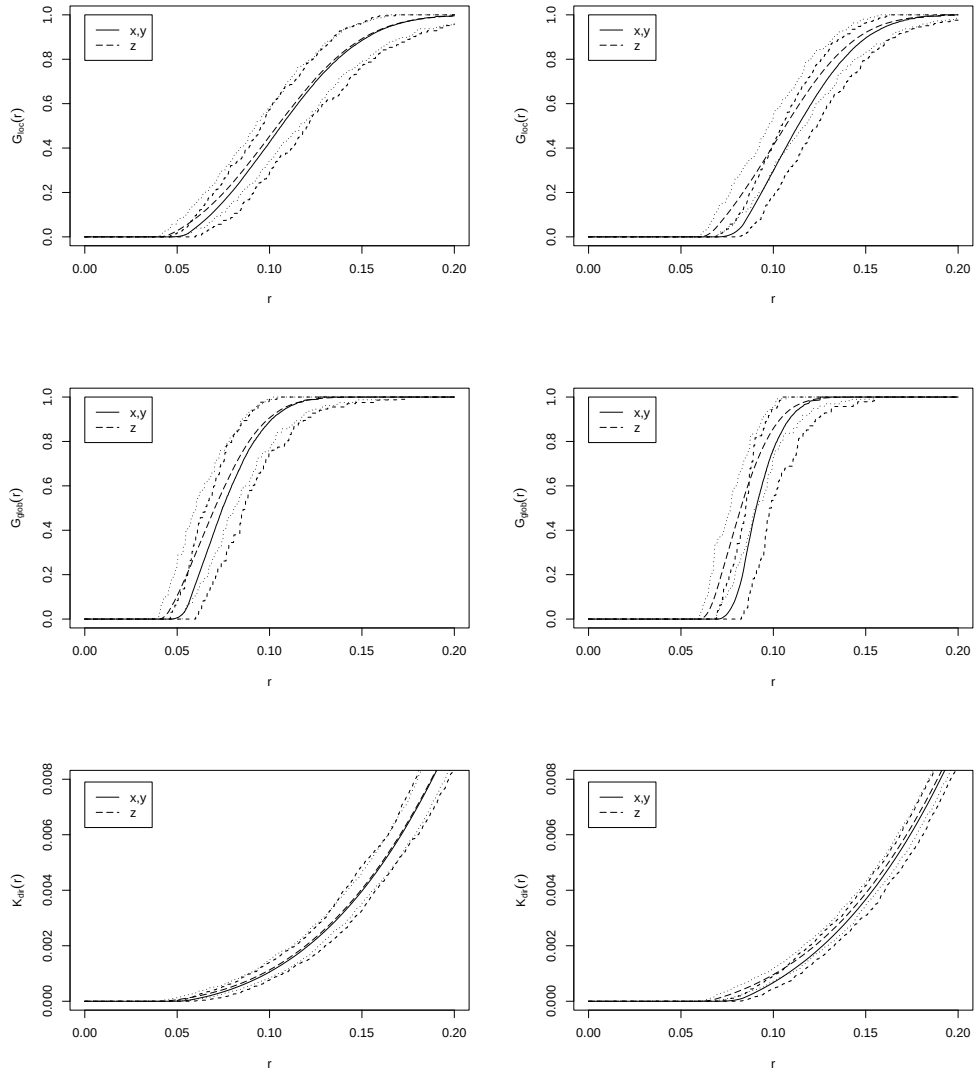

Figure 1: Means (solid for xy, dashed for z) and envelopes (short dashed for xy, dotted for z) of the functions G_{loc}, G_{glob}, and K_{dir} (from top to bottom) evaluated for 1000 realisations of a pressed Matérn hard core point process with the parameters $\lambda = 500$ and $R = 0.05$ (left) and $R = 0.075$ (right). The pressing factor is $c = 0.8$.

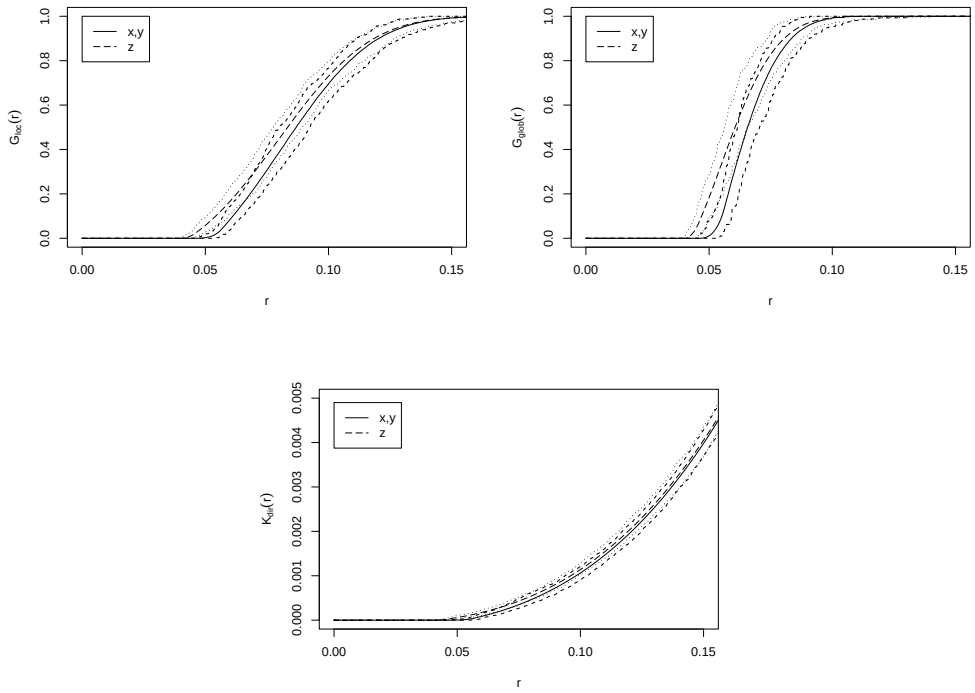

Figure 2: Means (solid for xy, dashed for z) and envelopes (short dashed for xy, dotted for z) of the functions G_{loc} (top left), G_{glob} (top right), and K_{dir} (bottom) evaluated for 1000 realisations of a pressed Matérn hard core point process with the parameters $\lambda = 1000$, $R = 0.05$. The pressing factor is $c = 0.8$.

Table 2: Powers of the isotropy tests using directional summary statistics on a 5% significance level for 1000 Matérn hard core point patterns of intensity $\lambda = 1000$ and hard core radius R pressed by the factor c. The test statistics were computed on the interval $[0, r_2]$.

c | R	0.025	0.025	0.025	0.05	0.05	0.05
0.9 | r_2	0.1	0.033	0.0275	0.1	0.067	0.055
G_{loc}	1.4	15.1	**59.3**	18.9	73.1	99.7
G_{glob}	1.9	**15.5**	58.8	**42.7**	71.1	99.8
K_{dir}	**2.1**	14.7	58.2	17.9	**79.7**	**100**
0.8 | r_2	0.1	0.033	0.0275	0.1	0.067	0.055
G_{loc}	1.3	53.2	87.0	84.4	**100**	**100**
G_{glob}	**4.2**	53.6	86.2	**97.1**	99.9	**100**
K_{dir}	2.6	**56.7**	**88.5**	77.6	**100**	**100**
0.7 | r_2	0.1	0.033	0.0275	0.1	0.067	0.055
G_{loc}	2.4	80.2	92.4	99.6	**100**	**100**
G_{glob}	**8.8**	80.1	91.5	**100**	**100**	**100**
K_{dir}	3.7	**82.5**	**93.7**	99.1	**100**	**100**

Table 3: Powers for the test based on λ_1 on a 5% significance level for 1000 Matérn hard core point patterns of intensity λ and hard core radius R pressed by the factor c.

λ	500	500	500	1000	1000
c | R	0.025	0.05	0.075	0.025	0.05
0.9	8.0	11.4	45.1	8.8	32.4
0.8	7.7	21.4	95.4	9.3	88.3
0.7	7.6	39.3	99.9	10.8	99.9

Table 4: Mean number of points used for the estimation of G_{loc} and G_{glob} for the point processes of intensity $\lambda = 500$ in the Matérn (M) and the force biased (FB) case.

	R	c	$G_{loc,x}$	$G_{loc,y}$	$G_{loc,z}$	$G_{glob,x}$	$G_{glob,y}$	$G_{glob,z}$
M	0.025	0.9	290.14	289.76	290.68	93.26	92.50	94.16
M	0.025	0.8	289.96	289.55	290.94	92.84	92.09	94.86
M	0.025	0.7	289.82	289.37	291.21	92.38	91.75	95.55
M	0.05	0.9	283.91	283.56	286.12	85.83	85.52	93.96
M	0.05	0.8	283.10	282.74	287.85	83.18	83.00	99.11
M	0.05	0.7	282.04	281.71	289.27	80.42	80.41	103.83
M	0.075	0.9	271.13	271.01	277.39	71.44	71.89	97.02
M	0.075	0.8	269.20	269.17	281.92	63.93	64.49	112.36
M	0.075	0.7	267.48	267.60	286.46	57.92	58.53	124.95
FB	0.05	0.9	267.06	266.84	270.01	72.49	72.97	91.84
FB	0.05	0.8	264.00	264.00	269.93	65.46	65.13	106.26
FB	0.05	0.7	259.83	259.34	267.10	57.70	57.09	120.20
FB	0.1	0.9	241.02	240.70	251.77	32.05	31.85	131.57
FB	0.1	0.8	237.64	237.37	258.71	12.81	12.78	183.13
FB	0.1	0.7	234.22	233.89	262.03	9.34	9.55	197.79

G_{glob} and a failure of the test.

4.2 Random packing of balls

To study also point patterns with a higher degree of regularity, we generated realisations of random packings of balls within the unit cube using the force biased algorithm (Bezrukov et al., 2001). This algorithm works with the concept of collective rearrangement. It starts with a fixed number of balls which are randomly placed inside a container. Overlaps are permitted in the initial configuration, but gradually reduced by shifting the balls and reducing their sizes. Throughout, the initial size distribution is preserved up to a scaling factor. Using this algorithm, dense packings of balls with arbitrary radius distributions may be generated.

Here, we are working with balls of equal size. Their radii were chosen as 0.025 and 0.05, yielding hard core radii of $R = 0.05$ and $R = 0.1$, respectively. For the distribution of the number of balls we chose a Poisson distribution with parameter $\lambda = 500$. As in the Matérn case, 1000 realisations were considered and the ball packings were scaled by the vector $(\frac{1}{\sqrt{c}}, \frac{1}{\sqrt{c}}, c)$ with $c = 0.7, 0.8$, and 0.9.

The envelopes of the directional summary statistics obtained in this case are shown in Figure 3. The difference between the curves for K_{dir} and G_{loc} is more pronounced, in contrast to the Matérn envelopes which are separated only close

Table 5: Powers of the isotropy tests using directional summary statistics on a 5% significance level for 1000 force biased packings of intensity $\lambda = 500$ and ball radius R pressed by the factor c. The test statistics were computed on the interval $[0, r_2]$.

c | R	0.05	0.05	0.05	0.1	0.1	0.1
0.9 | r_2	0.2	0.15	0.1	0.2	0.15	0.1
G_{loc}	**23.4**	27.1	14.9	**100**	**100**	51.4
G_{glob}	1.6	1.6	2.0	1.1	1.1	35.5
K_{dir}	13.4	**49.2**	**15.8**	**100**	**100**	**64.0**
0.8 | r_2	0.2	0.15	0.1	0.2	0.15	0.1
G_{loc}	85.2	87.0	63.8	**100**	**100**	97.3
G_{glob}	1.5	1.5	3.2	3.2	3.2	26.0
K_{dir}	**88.5**	**98.8**	**75.7**	**100**	**100**	**98.3**
0.7 | r_2	0.2	0.15	0.1	0.2	0.15	0.1
G_{loc}	99.2	99.5	97.3	**100**	**100**	**100**
G_{glob}	2.7	2.8	4.9	33.7	33.7	63.8
K_{dir}	**99.4**	**99.9**	**99.1**	**100**	**100**	**100**

to the hard core radius. For the larger hard core distance, the envelopes are even clearly disjoint over the whole interval of observation. Contrary, for G_{glob} the envelopes for xy and z are closer together which is due to the small number of points included in the statistics in this case (see Table 4). This suggests to work with K_{dir} or G_{loc} and to choose larger intervals for the anisotropy tests when working with more regular data.

The test results in Table 5 confirm this impression. The highest powers are obtained for K_{dir} followed by G_{loc} if both are evaluated on the intermediate interval. For $R = 0.1$ we observe powers of 100% for the anisotropy tests based on G_{loc} and K_{dir} for suitably large intervals. In contrast, the test based on G_{glob} yields only poor results.

4.3 Existence of outliers

The results presented so far indicate that the range of observation for the directional summary statistics should be chosen depending on both the degree of regularity and the hard core distance observed in a particular point pattern. A situation which is likely to appear in real data is the existence of outliers, i.e. few points in the pattern are permitted to violate the hard core condition.

In order to study the behaviour of the directional summary statistics in such cases we insert outliers in some of the simulated point patterns and repeat the analyses described above. For that purpose, five points $x_1, \ldots, x_5$ are chosen

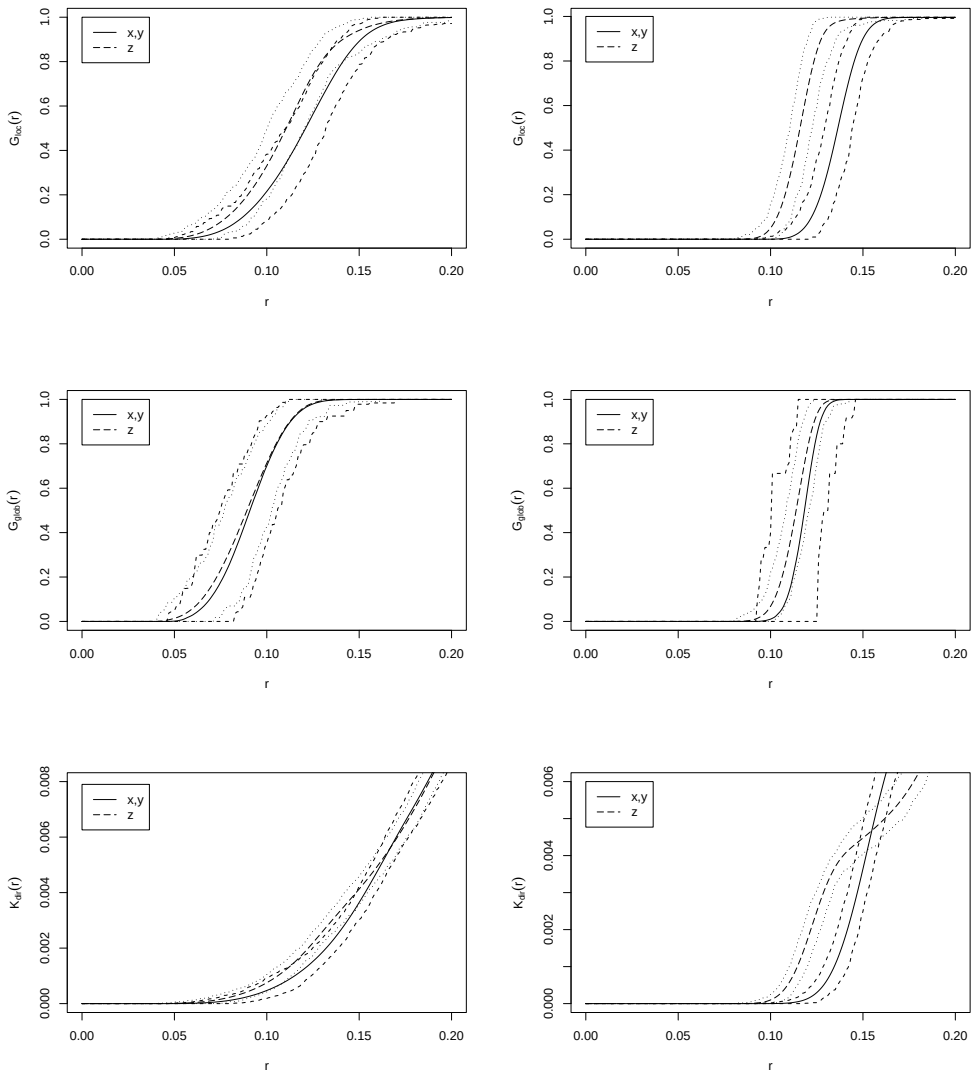

Figure 3: Means (solid for xy, dashed for z) and envelopes (short dashed for xy, dotted for z) of the functions G_{loc} (top left), G_{glob} (top right), and K_{dir} (bottom) evaluated for 1000 realisations of a pressed force biased packing with intensity $\lambda = 500$, hard core radius $R = 0.05$ (left) and $R = 0.1$ (right), and $c = 0.8$.

randomly from each point pattern. For each such point, an additional point y_i is generated from a uniform distribution on a ball of radius R centred in x_i. Then the directional summary statistics are estimated for the point patterns including the points $y_1, \ldots, y_5$. To keep the amount of simulations limited, the analysis is restricted to patterns of intensity $\lambda = 500$.

The envelopes obtained for the Matérn hard core processes and the force biased packings with $R = 0.05$ are shown in Figure 4. In the Matérn case, the envelopes for the (x, y)- and the z-direction are no longer separated. Even in the pure hard core case this was only the case for values of r close to the hard core distance, exactly in the area which is most affected by the existence of outliers. The curves for the force biased packings show similar changes for values close to R. Nevertheless, we might still expect acceptable power of the tests, since the results in the previous section suggested to use larger intervals in this case. The most striking changes are visible in the envelopes for G_{glob} which is strongly influenced by the existence of outliers.

The powers of the isotropy tests are given in Tables 6 and 7. From the observation of the envelopes decreasing powers can be expected in the presence of outliers. Especially for G_{glob}, this indeed turns out to be the case. Besides this decrease, the results for the larger hard core radius $R = 0.075$ look similar to the results in the pure hard core case. On the interval $[0, 0.2]$ the G functions yield better results, while on both other intervals as well as in the total, K_{dir} performs best. For the smaller hard core radius $R = 0.05$ the situation is different. Now the best results for each of the functions are obtained using the intermediate interval since the structure of the curves for r close to the hard core radius R is mainly governed by the outliers. Again, the test based on K_{dir} yields the best total value.

In the force biased case the powers behave as expected, too. At least on the two larger intervals we obtain similar values as in the non-outlier case.

5 Estimation of the pressing factor

We have seen that the anisotropy tests work well if both the intensity of the point pattern and the hard core radius are sufficiently large. Now we are going to investigate, whether the statistics can also be used for the estimation of the pressing parameter c. For that purpose, we simulate 100 realisations of Matérn hard core point processes and force biased packings with parameters as in Section 4. Each realisation is pressed using the pressing factors $c = 0.7, 0.8, 0.9$, and 1.0. Then, every pattern is rescaled by the vector $(\sqrt{d}, \sqrt{d}, \frac{1}{d})$, where d takes values between 0.6 and 1.1 at steps of 0.025. If the values of c and d are similar, both operations cancel out and the resulting pattern is close to the original, hence

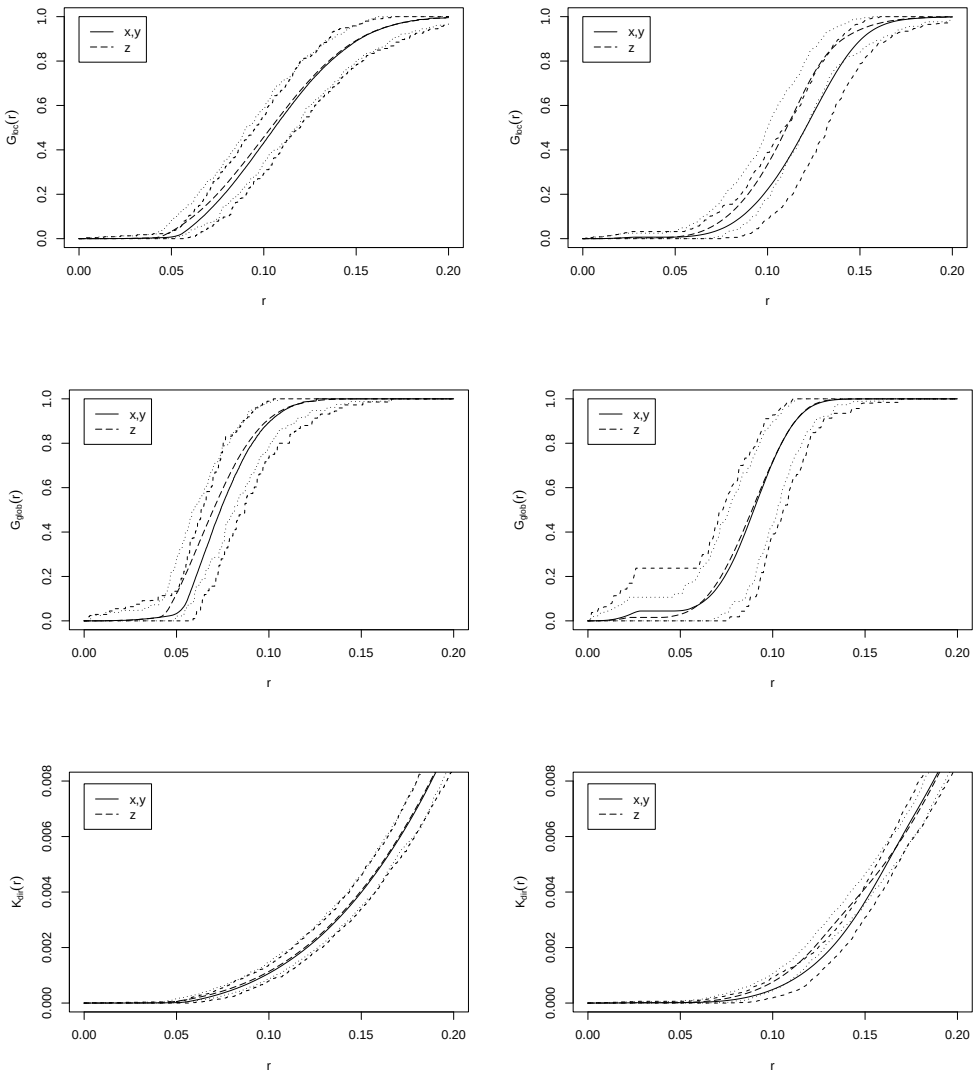

Figure 4: Means (solid for xy, dashed for z) and envelopes (short dashed for xy, dotted for z) of the functions G_{loc}, G_{glob}, and K_{dir} (from top to bottom) evaluated for 1000 realisations of pressed Matérn hard core point processes (left) and force biased packings (right) of intensity $\lambda = 500$ with five outliers. The hard core radius is $R = 0.05$, the pressing factor is $c = 0.8$.

Table 6: Powers of the isotropy tests using directional summary statistics on a 5% significance level for 1000 Matérn hard core point patterns of intensity $\lambda = 500$ and hard core radius R including five outliers and pressed by the factor c. The test statistics were computed on the interval $[0, r_2]$.

c | R	0.05	0.05	0.05	0.075	0.075	0.075
0.9 | r_2	0.1	0.067	0.055	0.2	0.1	0.0825
G_{loc}	2.8	10.4	**6.7**	14.1	56.2	81.8
G_{glob}	**3.9**	6.4	2.4	**23.1**	29.5	25.4
K_{dir}	3.3	**10.6**	5.0	6.0	**63.8**	**87.8**
0.8 | r_2	0.1	0.067	0.055	0.2	0.1	0.0825
G_{loc}	**13.7**	49.6	**45.1**	67.2	98.1	**100**
G_{glob}	**13.7**	30.6	17.2	**75.3**	84.3	79.3
K_{dir}	11.1	**54.3**	39.5	22.6	**99.4**	**100**
0.7 | r_2	0.1	0.067	0.055	0.2	0.1	0.0825
G_{loc}	**34.5**	77.8	68.3	**96.1**	**100**	**100**
G_{glob}	29.8	57.1	35.0	93.3	95.3	90.2
K_{dir}	33.4	**81.7**	**70.1**	65.1	**100**	**100**

Table 7: Powers of the isotropy tests using directional summary statistics on a 5% significance level for 1000 force biased packings of intensity $\lambda = 500$ and hard core radius R including five outliers and pressed by the factor c. The test statistics were computed on the interval $[0, r_2]$.

c | R	0.05	0.05	0.05	0.1	0.1	0.1
0.9 | r_2	0.2	0.15	0.1	0.2	0.15	0.1
G_{loc}	**23.9**	26.1	9.2	**100**	**100**	0.5
G_{glob}	0.5	0.5	0.6	0.1	0.1	0.1
K_{dir}	11.0	**44.2**	**9.6**	**100**	**100**	**0.6**
0.8 | r_2	0.2	0.15	0.1	0.2	0.15	0.1
G_{loc}	**82.2**	84.7	50.9	**100**	**100**	0.8
G_{glob}	0.0	0.0	0.0	0.1	0.1	0.1
K_{dir}	81.4	**97.9**	**58.5**	**100**	**100**	**1.3**
0.7 | r_2	0.2	0.15	0.1	0.2	0.15	0.1
G_{loc}	**98.9**	**99.0**	93.4	**100**	**100**	64.8
G_{glob}	0.1	0.1	0.1	0.0	0.0	0.1
K_{dir}	98.5	**99.0**	**97.6**	**100**	**100**	**96.7**

isotropic. For large differences between c and d, however, the resulting pattern will show a certain degree of anisotropy which can be detected by our methods.

For each of the rescaled patterns we compute the statistic $T_{\sum,d}$ (the statistic $T_{\sum}$ for the pattern rescaled by the factor d) based on all three summary statistics introduced above using two different choices of the integration interval: $[0, 1.1R]$ and $[0, \frac{4R}{3}]$ in the Matérn case and $[0, 0.15]$ and $[0, 0.2]$ for the force biased packings. The statistic $T_{\sum}$ was chosen here rather than a statistic based on T_z or T_{xy}, since it allows for a simultaneous measurement of the deviation between all three directions. Now $\hat{c} = \text{argmin}_d\, T_{\sum,d}$, i.e. the value of d leading to the most isotropic patterns, is considered as estimator for the pressing factor c.

The means of the estimated values and the mean squared error (MSE) of the estimation are displayed in Tables 8 and 9. Only the values for the interval yielding the smaller MSE are shown. In most of the cases, this turned out to be the smaller interval. In general, the trends observed in the testing part are confirmed in this study. The MSE for the estimates is smaller for higher intensities and higher degrees of regularity and in most of the cases K_{dir} yields the best results. Only in some of the Matérn examples the degree of compression does not influence the estimation results as significantly as in the testing part. When interpreting the results one should keep in mind that the MSE is also influenced by the choice of the d values considered.

6 Application to the ice data

We now apply our estimation methods to ice samples from an ice core which was drilled during an ongoing deep drilling project at Talos Dome, Antarctica (159°04′ E, 72°46′ S). The achieved drilling depth after the season 2006/2007 is about 1600 m, only slightly less than the predicted absolute ice thickness. The accumulation rate is estimated to about 100 mm water equivalent per year in the Thalos Dome region (Stenni et al. (2002)).

Three different depths between the firn-ice transition and the transition of bubbly to clathrate ice are chosen: 153 m, 353 m, and 505 m depth. For each depth 14 samples are prepared to cover the structural variations on the centimetre scale as the amount of bubbles per volume ice is fluctuating on the small scale. The fluctuations correspond to variations in grain size at the firn-ice transition caused by seasonal variations in surface snow properties and snow fall events.

The samples are imaged by X-ray microfocus computer tomography (μCT) using a μCT-1072 (Skyscan, Belgium) inside a cold room at -15 °C. The sample size is limited to cylinders of 15 mm diameter and 15 mm height. Therefore the ice is cut into cubes of 2 cm side length and rasped on a rotating turn table to form regular cylinders. The scanning volume is adjusted to the specific sample

Table 8: Means of the estimated pressing factors $\hat{c}_K$, $\hat{c}_{G_{\mathrm{loc}}}$, and $\hat{c}_{G_{\mathrm{glob}}}$ for the Matérn point patterns and MSE of the estimation.

λ	R	r_2	c	$\hat{c}_{\mathrm{loc}}$	MSE	$\hat{c}_{\mathrm{glob}}$	MSE	$\hat{c}_K$	MSE
1000	0.05	0.055	1.0	0.9988	5.813e-4	0.9995	7.625e-4	0.9993	**4.063e-4**
1000	0.05	0.055	0.9	0.8985	4.375e-4	0.8985	4.750e-4	0.8988	**3.438e-4**
1000	0.05	0.055	0.8	0.7988	**3.438e-4**	0.8018	5.313e-4	0.7990	4.125e-4
1000	0.05	0.055	0.7	0.6993	4.313e-4	0.6990	4.125e-4	0.6998	**3.938e-4**
1000	0.025	0.033	1.0	0.9480	1.513e-2	0.9513	1.596e-2	0.9590	**1.154e-2**
1000	0.025	0.033	0.9	0.8745	1.335e-2	0.8858	**1.071e-2**	0.8950	1.270e-2
1000	0.025	0.033	0.8	0.8248	**1.141e-2**	0.8250	1.360e-2	0.8285	1.290e-2
1000	0.025	0.0275	0.7	0.6865	7.325e-3	0.6820	7.038e-3	0.6923	**6.769e-3**
500	0.075	0.0825	1.0	1.0000	5.625e-4	1.0000	5.375e-4	0.9988	**5.063e-4**
500	0.075	0.0825	0.9	0.8955	5.250e-4	0.8968	7.438e-4	0.8973	**4.563e-4**
500	0.075	0.0825	0.8	0.7973	4.438e-4	0.7945	9.625e-4	0.7980	**4.375e-4**
500	0.075	0.0825	0.7	0.6978	5.063e-4	0.7003	5.813e-4	0.6963	**4.813e-4**
500	0.05	0.055	1.0	0.9828	**3.944e-3**	0.9795	6.763e-3	0.9875	4.850e-3
500	0.05	0.055	0.9	0.8810	5.813e-3	0.8855	5.138e-3	0.8933	**3.631e-3**
500	0.05	0.055	0.8	0.7780	5.363e-3	0.7818	4.544e-3	0.7923	**2.844e-3**
500	0.05	0.055	0.7	0.6880	**1.850e-3**	0.6913	1.981e-3	0.6860	1.988e-3
500	0.025	0.033	1.0	0.8270	6.264e-2	0.8285	6.020e-2	0.8335	**5.733e-2**
500	0.025	0.033	0.9	0.8158	3.473e-2	0.8210	**3.291e-2**	0.8200	3.335e-2
500	0.025	0.033	0.8	0.7678	2.299e-2	0.7860	2.364e-2	0.7708	**2.037e-2**
500	0.025	0.0275	0.7	0.6263	9.981e-3	0.6245	**9.663e-3**	0.6263	1.00e-2

Table 9: Means of the estimated pressing factors $\hat{c}_K$, $\hat{c}_{G_{\mathrm{loc}}}$, and $\hat{c}_{G_{\mathrm{glob}}}$ for force biased packings with m outliers and MSE of the estimation.

λ	R	m	r_2	c	$\hat{c}_{\mathrm{loc}}$	MSE	$\hat{c}_{\mathrm{glob}}$	MSE	$\hat{c}_K$	MSE
500	0.1	0	0.15	1.0	1.0005	2.000e-4	1.0130	4.200e-3	0.9983	**1.063e-4**
500	0.1	0	0.15	0.9	0.8998	1.438e-4	0.9290	5.763e-3	0.8985	**7.500e-5**
500	0.1	0	0.15	0.8	0.7995	1.000e-4	0.8378	7.806e-3	0.7990	**6.250e-5**
500	0.1	0	0.15	0.7	0.6998	4.375e-5	0.7358	8.419e-3	0.6995	**1.250e-5**
500	0.1	5	0.15	1.0	0.9988	1.938e-4	1.0103	3.806e-3	0.9980	**1.125e-4**
500	0.1	5	0.15	0.9	0.8988	1.563e-4	0.9320	6.150e-3	0.8990	**6.250e-5**
500	0.1	5	0.15	0.8	0.7990	1.250e-4	0.8470	1.095e-2	0.7993	**3.125e-5**
500	0.1	5	0.15	0.7	0.6993	4.375e-5	0.7660	1.805e-2	0.6995	**2.500e-5**
500	0.05	0	0.15	1.0	1.0005	2.625e-3	0.9385	2.081e-2	0.9955	**1.813e-3**
500	0.05	0	0.15	0.9	0.8953	2.806e-3	0.9060	1.819e-2	0.8993	**1.669e-3**
500	0.05	0	0.15	0.8	0.7968	2.306e-3	0.8655	2.511e-2	0.8030	**1.013e-3**
500	0.05	0	0.15	0.7	0.6958	1.631e-3	0.8128	3.222e-2	0.7015	**7.125e-4**
500	0.05	5	0.15	1.0	0.9920	3.163e-3	0.9195	2.649e-2	1.0018	**1.819e-3**
500	0.05	5	0.15	0.9	0.9023	3.294e-3	0.8705	2.038e-2	0.9025	**1.775e-3**
500	0.05	5	0.15	0.8	0.8033	2.594e-3	0.8745	3.070e-2	0.8043	**1.444e-3**
500	0.05	5	0.15	0.7	0.6995	2.088e-3	0.8188	3.722e-2	0.6990	**1.013e-3**

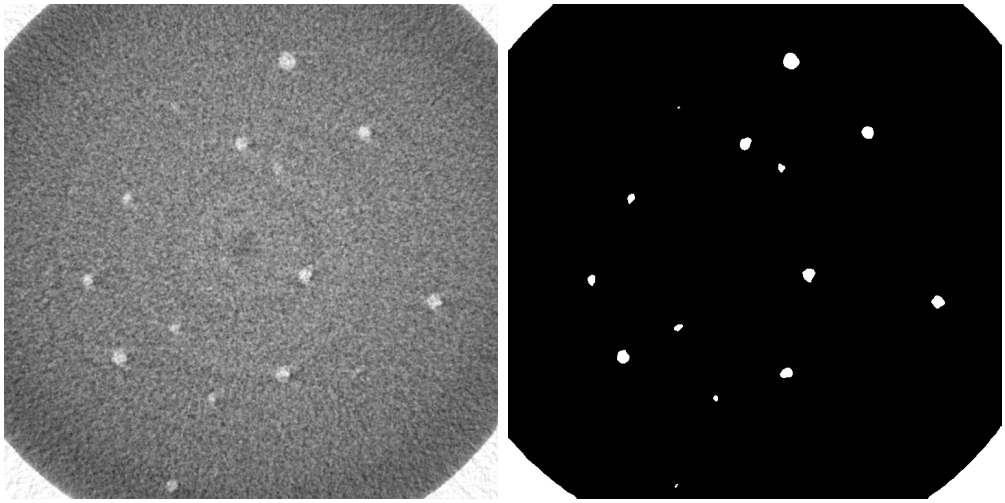

Figure 5: 2d sections of the original (left) and the binarised (right) image of an ice sample from depth 353 m.

size by varying the spatial resolution between 13 and 16 μm per pixel. For each sample a digital reconstruction algorithm generates a set of 900 images of 1024 x 1024 pixels.

In this paper, we restrict attention to the samples taken from 353 m and 505 m depth. Due to the large difference in X-ray absorption between air and ice, the volume images are simply segmented by global thresholding to identify air bubbles in the ice matrix (see Figure 5). A subsequent labelling algorithm allows to distinct the single bubbles and to compute their centres. For the estimation of the summary statistics, cuboidal observation windows are fitted into the cylinders and all pore centres contained in the cuboids are extracted. In order to find the maximal number of pores for each sample, the observation windows are not required to have equal size. Only objects with a volume larger than 25 voxels are included in the analysis yielding point patterns containing between 329 and 733 points. All image processing steps are performed on volume images using the MAVI software package (Fraunhofer ITWM, 2005). Figure 6 shows visualisations of one sample from each depth.

In contrast to the simulated data, the pore intensities in different ice samples cannot be assumed to be the same due to the variations on the centimetre scale. Therefore, we use the ratio estimation method described in Baddeley et al. (1993) to pool the summary statistics within the depths. This means that the mean

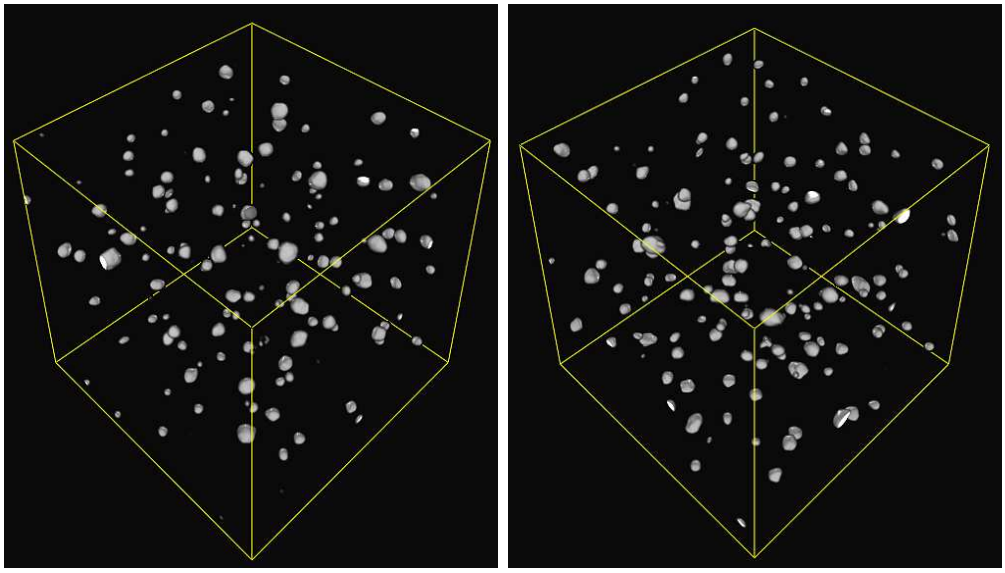

Figure 6: Visualisations of the system of air pores in ice samples from depth 353 m (left) and 505 m (right).

curves are estimated as

$$\hat{S} = \frac{\sum_{i=1}^{14} U_i}{\sum_{i=1}^{14} V_i}.$$

For K_{dir}, U_i is the double sum in (1) and V_i is the estimated squared intensity evaluated for sample i. For the G functions, U_i and V_i are the numerators and denominators, respectively, in (2) and (3). Scatter plots of U_i against V_i, which are not shown here, indicated that the assumption of a linear relation between these numbers is justified. Confidence bands at a 95% level were computed using the sample variances and the quantiles of the t-distribution with 13 degrees of freedom. The means and confidence bands of the directional summary statistics G_{loc}, G_{glob}, and K_{dir} for the ice samples are shown in Figure 7. Especially for G_{loc} and K_{dir}, a clear deviation between the confidence bands for the (x, y)- and the z-direction is observed. Therefore, the hypothesis of isotropy can clearly be rejected in this case.

For the estimation of the pressing factors, we have to choose a suitable interval of integration. Therefore, we first investigate the degree of regularity of the pore system by estimating the isotropic pair-correlation function of the point patterns of pore centres. The results for five samples from each depth are shown in Figure 8. The wave-like appearance of the curves resembles the structure

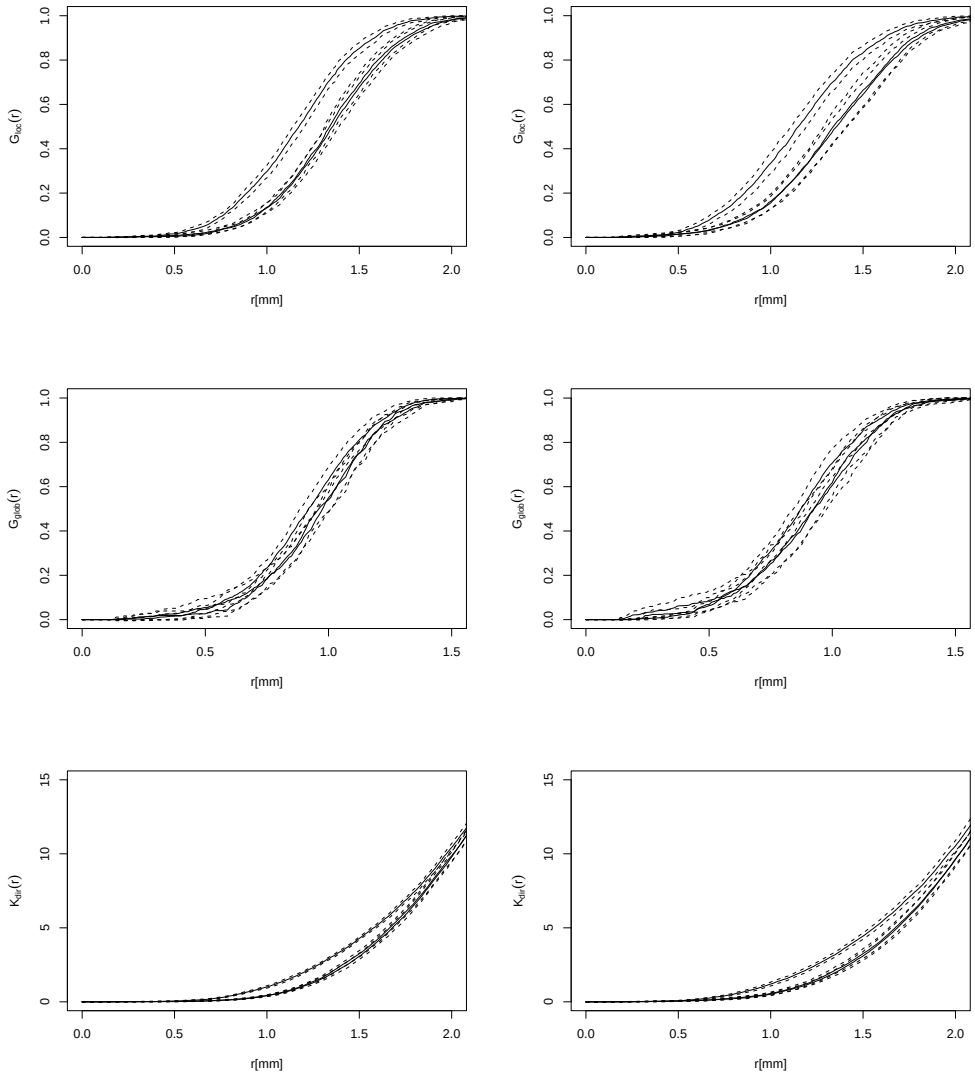

Figure 7: Means and confidence bands of the functions G_{loc}, G_{glob}, and K_{dir} (from top to bottom) evaluated for the ice samples from depth 353 m (left) and 505 m (right).

which is typically observed in pair-correlation functions of dense packings of balls (Stoyan et al., 1995). This is an evidence for a very regular structure of the data.

The histograms of the nearest neighbour distances for three samples per depth are shown in Figure 9. The gaps on the left tail of the histograms indicate the existence of outliers in the ice samples.

Combined with the results of our simulation studies, these observations suggest the choice of an intermediate interval size for the estimation of the pressing factors as well as the use of G_{loc} or K_{dir} rather than G_{glob}. The confidence bands shown in Figure 7 are clearly separated over the whole interval $[0, 2.0]$. Therefore, we decided to choose $[0, 2.0]$ for the estimation of the pressing factors, which allows to control the behaviour of the functions over the whole range. For the rescaling of the samples from depth 353 m, we used values of d ranging between 0.5 and 1.0 at steps of 0.025. Since stronger pressing is expected in deeper areas, the values for the samples from depth 505 m were chosen between 0.3 and 0.8. The estimates $\hat{c}_G$ and $\hat{c}_K$ obtained using G_{loc} and K_{dir} are given in Table 10. They confirm that the compression of the ice is stronger at the depth 505 m than at 353 m depth.

In order to investigate the estimation variance in this case, we adopt a bootstrap method as described in Illian et al. (2008, p.454). For each of the two summary statistics and depths, 200 new samples of $\hat{c}$ values are generated by random resampling from the estimated values with replacement. The estimation variance is then approximated by the sample variance of their means. For depth 353 m, we obtained values of $3.045 \cdot 10^{-4}$ (G_{loc}) and $1.667 \cdot 10^{-4}$ (K_{dir}), the values for 505 m are $9.341 \cdot 10^{-5}$ (G_{loc}) and $2.543 \cdot 10^{-4}$ (K_{dir}). The corresponding 95% confidence intervals are disjoint for the two depths considered. They are

$$\begin{array}{lll} 353\mathrm{m}: & (0.607, 0.679) \text{ using } G_{\mathrm{loc}} & \text{and } (0.604, 0.655) \text{ using } K_{\mathrm{dir}}, \text{ and} \\ 505\mathrm{m}: & (0.518, 0.577) \text{ using } G_{\mathrm{loc}} & \text{and } (0.516, 0.552) \text{ using } K_{\mathrm{dir}}. \end{array}$$

In order to further evaluate the estimates, the mean curves of G_{loc} and K_{dir} for the rescaled point patterns are shown in Figure 10. For both functions, the difference between the (x, y)- and the z-direction turns out to be small in the rescaled patterns.

7 Discussion

The main aim of the paper was to study anisotropy of air pores in polar ice. The hypothesis is that the ice is compressed and therefore, the spatial pattern of the air pores in z-direction differs from the pattern in x- or y-direction. To investigate this, we introduced some directional summary statistics in 3D based on the nearest neighbour distance distribution function and Ripley's K function.

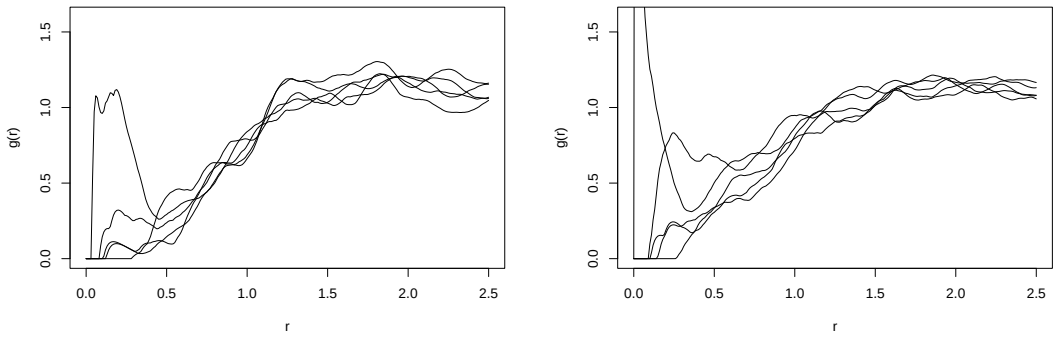

Figure 8: Isotropic pair correlation functions estimated for five ice samples taken from depth 353 m (left) and 505 m (right).

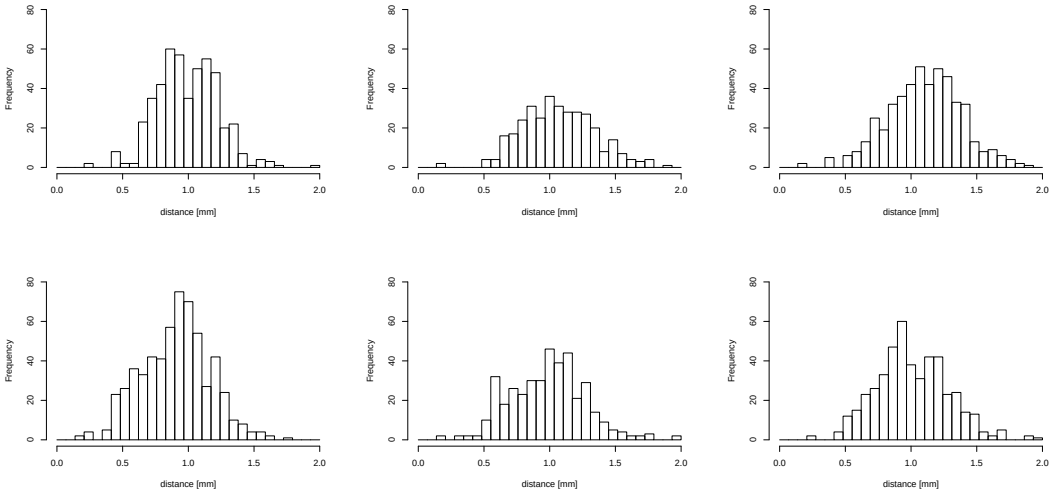

Figure 9: Histograms of distances to the nearest neighbours for three samples from depth 353 m (top) and 505 m (bottom).

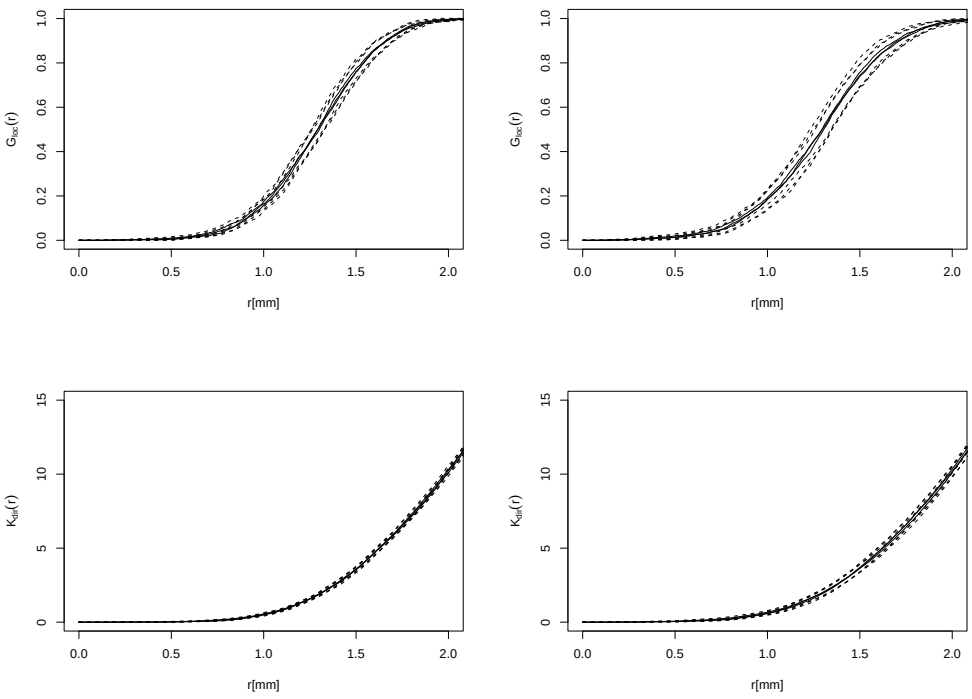

Figure 10: Means (solid) and confidence bands (dashed) of the functions G_{loc} (top) and K_{dir} (bottom) for the rescaled versions of the ice samples using the estimated pressing factors $\hat{c}_G$ and $\hat{c}_K$, respectively. The samples from depth 353 m are shown on the left, the samples from depth 505 m on the right.

Table 10: Results for the ice samples: number of pores n, pores per volume N_V, and the pressing factors $\hat{c}_G$ and $\hat{c}_K$ estimated using G_{loc} and K_{dir}, respectively.

353 m	n	N_V	$\hat{c}_G$	$\hat{c}_K$	505 m	n	N_V	$\hat{c}_G$	$\hat{c}_K$
1	411	0.3511	0.575	0.575	1	675	0.3559	0.500	0.575
2	431	0.3228	0.550	0.550	2	733	0.4414	0.550	0.500
3	398	0.2981	0.625	0.625	3	549	0.2937	0.500	0.700
4	478	0.3906	0.675	0.675	4	639	0.4310	0.550	0.525
5	411	0.4019	0.625	0.625	5	590	0.4398	0.500	0.625
6	439	0.3861	0.675	0.600	6	398	0.3063	0.500	0.500
7	372	0.3125	0.650	0.575	7	356	0.2682	0.550	0.525
8	334	0.2938	0.550	0.575	8	439	0.2761	0.575	0.500
9	369	0.3246	0.575	0.600	9	493	0.2969	0.600	0.525
10	329	0.3907	0.650	0.775	10	463	0.2870	0.500	0.475
11	550	0.3220	0.650	0.750	11	479	0.2885	0.500	0.550
12	485	0.2754	0.700	0.725	12	466	0.2931	0.575	0.575
13	649	0.3577	0.650	0.650	13	541	0.3357	0.575	0.575
14	711	0.3318	0.675	0.675	14	413	0.2715	0.500	0.475
mean	454.79	0.3403	0.630	0.641	mean	516.71	0.3241	0.534	0.545

These summary statistics were used to develop tests for isotropy against this specific type of anisotropy. An adaptation of the methods for the detection of anisotropies with respect to other directions is straightforward.

The tests presented here are based on replicates, and have the advantage that there is no need to assume and fit a model to the data. In a simulation study we evaluated the powers of the tests for regular patterns of different intensities, degrees of regularity, and strengths of compression. As expected, the best results (highest powers) were obtained with high intensities, high degrees of regularity (e.g. large hard-core radii) and strong pressing. For Matérn hard core point processes, the test based on the directional K function performed best. The size of the interval of observation should be chosen depending on the hard core distance. However, it turned out that tests based on the G functions are more robust to changes of this interval. For point processes with a high degree of regularity, such as packings of balls, the use of the K function or the local G function on a larger interval is recommended. In this case, our methods also proved robust to the existence of outliers. In the point process literature it is often suggested to use more than one summary statistic for the analysis of a point pattern. Despite the better test results for K_{dir} it seems therefore advisable to work with both K_{dir} and G_{loc}.

If only a few replicates are available, it is possible to perform a Monte Carlo tests based on the summary statistics presented here. In this case, it is necessary to find an appropriate model for the data in order to be able to simulate patterns from it. The results based on the Monte Carlo test are similar to the results based

on the data based tests, when testing on simulated data. If the regularity in the data is not very pronounced, one has to be careful when determining the hard core distance, since it affects the choice of the interval on which the differences between the summary statistics in different directions are investigated.

In addition to the summary statistics we have considered here, the distribution of the distances not only to the nearest neighbour but to all other points in the pattern could be investigated. This function is closely related to the point-pair-rose-density. The advantage of using all points is discussed in a paper by Fry (1979) on strain measurement in rocks. For the estimation of this function, only distances up to a maximal value should be considered. Depending on how large this value is chosen, an edge correction similar to the ones for the G functions would result in estimates based on either a small number of points with a lot of information or a large number of points with little information. It is not clear in advance, which alternative should be preferred.

We performed a simulation study for regular patterns with hard core since the air pore patterns are regular. However, it is also interesting to investigate how the tests work for clustered patterns. In this case, the aim is a detection of a change of the shapes of clusters caused by the pressing. We performed a simulation study also for Matérn cluster processes even though the results are not reported here. As in the hard core case, both high intensities and large pressing factors yield high powers of the test. In contrast to the regular case, anisotropies within point patterns with small cluster radii are easier to detect than within patterns with large cluster radii, since the concentration of points within the clusters is higher. Also, it turns out that the tests work better in the case of less points in a cluster. As in the regular case, the test based on the K function works best followed by the local G function while the global G function yields only poor results.

For the analysis of the ice samples not only the detection of anisotropies was required but also the measurement of its strength. In order to study this, we introduced a method to estimate the pressing factor. The observed pattern is 'stretched' using different pressing factors. The factor minimizing the difference between the spatial structure in the three coordinate directions, hence yielding the most isotropic pattern, is chosen as the estimate of the pressing factor. The evaluation of the estimation procedure on simulated data produced satisfactory results. Especially for very regular patterns the method works very well even in the presence of outliers.

Applied to the ice data, our methods render the anisotropy in z-direction caused by the compression of the ice sheet clearly visible. The means of the estimated pressing factors of 0.63/0.64 for the samples from 353 m depth and 0.53/0.55 for the depth of 505 m are consistent with the expected increase of the degree of compression with increasing depth. For the samples from 153 m depth we obtained mean pressing factors of 0.81/0.82 which confirms this finding.

However, the comparison of the mean curves for the two depths shown in Figure 11 indicate further structural differences between samples from different depths. A detailed investigation of these questions including samples from further depths is subject to future research.

A simple model of ice flow known as Nye formula in the glaciological literature (described in Paterson (1994)) assumes a constant thinning rate with depth. The Nye-approach is fairly simple and needs only the absolute ice thickness as an input parameter. Assuming an ice thickness of about 1600 m for Talos Dome one gets thinning factors of 0.90 (153 m), 0.78 (353 m) and 0.68 (505 m). Our estimations show an excellent agreement in the relative trend but with an absolute offset of about 0.1. One possible reason might be the oversimplification of the Nye-approach. It takes neither the bedrock boundary conditions nor the change of mechanical properties of ice with age and climate into account. The absolute thinning factor is very sensitive against the bedrock conditions. An assumed freezing at the bedrock would shift the absolute values in the upper part of the ice sheet towards higher thinning factors. Simulations with the so called Dansgaard-Johnsen approach (also described in Paterson (1994)) which parametrised the effect of bedrock freezing with a linear decrease of the thinning rate to zero at bedrock results in absolute thinning factors comparable to our estimations. However, the parametrisation of the linear decrease is arbitrary in the model and the real bedrock conditions at the Talos Dome site are not known due to the incomplete drilling so far. However, the qualitative agreement with the pure constrained model representations gives us confidence that the dating of ice cores will benefit from the independent estimations of the thinning function in future.

Acknowledgements

We would like to thank Björn Wagner for assistance with the image processing. Claudia Lautensack and Aila Särkkä acknowledge support by the Swedish Foundation for Strategic Research (SSF) through the Gothenburg Mathematical Modelling Centre (GMMC).

This work is a contribution to the Talos Dome Ice core Project (TALDICE), a joint European programme, funded by national contributions from Italy, France, Germany, Switzerland and the United Kingdom. The main logistic support was provided by PNRA. This is TALDICE publication no. XX.

References

ANDERSON, T. W. and M. A. STEPHENS (1972), Tests for randomness of

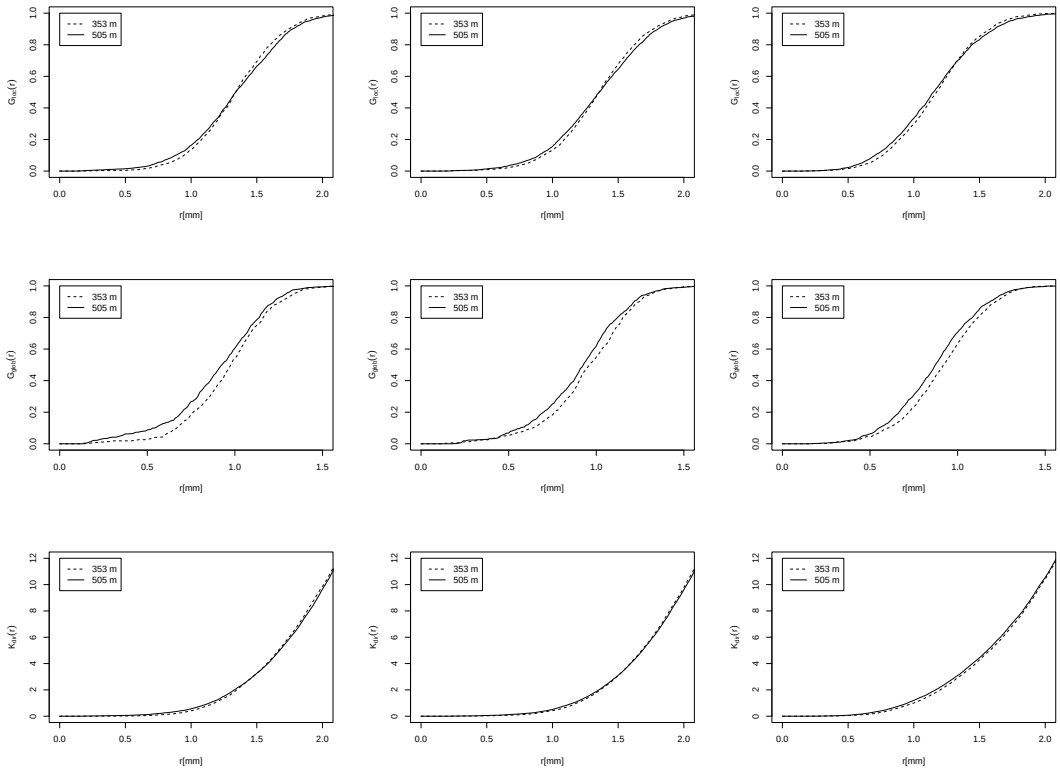

Figure 11: Comparison of the directional summary statistics for the ice samples from depths 353 m and 505 m. Means of the functions G_{loc}, G_{glob}, and K_{dir} (from top to bottom) evaluated for the x-, y-, and z-direction (from left to right).

directions against equatorial and bimodal alternatives, *Biometrika 59*(3), 613–621.

BADDELEY, A. J., R. A. MOYEED, C. HOWARD and A. BOYDE (1993), Analysis of a three-dimensional point pattern with replication, *Applied Statistics 42*, 641–668.

BENDER, M., T. SOWERS, M.-L. DICKSON, J. ORCHADO, P. GROOTES, P. A. MAYEWSKI and D. A. MEESE (1994), Climate correlations between Greenland and Antarctica during the past 100,000 years, *Nature 372*, 663–666.

BEZRUKOV, A., M. BARGIEL and D. STOYAN (2001), Statistical analysis of simulated random packings of spheres, *Particle & Particle Systems Characterization 19*, 111–118.

DIGGLE, P. (2003), *Statistical analysis of spatial point patterns*, Academic Press, London.

DUVAL, P. (2000), Deformation and dynamic recrystallization of ice in polar ice sheets, in: T. HONDOH (Ed.), Physics of ice core records, Hokkaido University Press.

EPICA community members, L. Augustin, C. Barbante, P. Barnes, J.-M. Barnola, M. Bigler, E. Castellano, O. Cattani, J. Chappellaz, D. Dahl-Jensen, B. Delmonte, G. Dreyfus, G. Durand, S. Falourd, H. Fischer, J. Flckiger, M. E. Hansson, P. Huybrechts, G. Jugie, S. Johnsen, J. Jouzel, P. Kaufmann, S. Kipfstuhl, F. Lambert, V. Lipenkov, G. C. Littot, A. Longinelli, R. Lorrain, V. Maggi, V. Masson-Delmotte, H. Miller, R. Mulvaney, J. Oerlemans, H. Oerter, G. Orombelli, F. Parrenin, D. A. Peel, J.-R. Petit, D. Raynaud, C. Ritz, U. Ruth, J. Schwander, U. Siegenthaler, R. Souchez, B. Stauffer, J. P. Steffensen, B. Stenni, T. F. Stocker, I. E. Tabacco, R. Udisti, R. S. W. van de Wal, M. van den Broeke, J. Weiss, F. Wilhelms, J.-G. Winther, E. Wolff and M. Zucchelli (2004), Eight glacial cycles from an antarctic ice core, *Nature 429*, 623–628.

EPICA community members, C. Barbante, J.-M. Barnola, S. Becagli, J. Beer, M. Bigler, C. Boutron, T. Blunier, E. Castellano, O. Cattani, J. Chappellaz, D. Dahl-Jensen, M. Debret, B. Delmonte, D. Dick, S. Falourd, S. Faria, U. Federer, H. Fischer, J. Freitag, A. Frenzel, D. Fritzsche, F. Fundel, P. Gabrielli, V. Gaspari, R. Gersonde, W. Graf, D. Grigoriev, I. Hamann, M. A. Hutterli, P. Huybrechts, E. Isaksson, S. Johnsen, J. Jouzel, M. Kasczmarska, T. Karlin, P. Kaufmann, S. Kipfstuhl, M. Kohno, F. Lambert, A. Lambrecht, A. Landais, G. Lawer, M. Leuenberger, G. Littot, L. Loulergue, D. Lthi,

V. Maggi, F. Marino, V. Masson-Delmotte, H. Meyer, H. Miller, R. Mulvaney, B. Narcisi, J. Oerlemans, H. Oerter, F. Parrenin, J.-R. Petit, G. Raisbeck, D. Rayaud, R. Rthlisberger, U. Ruth, O. Rybak, M. Severi, J. Schmitt, J. Schwander, U. Siegenthaler, M.-L. Siggaard-Andersen, R. Spahni, J. P. Steffensen, B. Stenni, T. F. Stocker, J.-L. Tison, R. Traversi, R. Udisti, F. Valero-Delgado, M. van de Broeke, R. S. W. van der Wal, D. Wagenbach, A. Wegner, K. Weiler, F. Wilhelms, J.-G. Winther and E. W. Wolff (2006), One-to-one coupling of glacial climate variability in Greenland and Antarctica, *Nature 444*, 195–198.

FRAUNHOFER ITWM (2005), MAVI – Modular Algorithms for Volume Images, www.mavi-3d.de

FRY, N. (1979), Random point distributions and strain measurement in rocks, *Tectonophysics 60*, 89–105.

HANISCH, K.-H. (1984), Some Remarks on Estimators of the Distribution Function of Nearest Neighbour Distance in Stationary Spatial Point Processes, *Mathematische Operationsforschung und Statistik, Series statistics 15*(3), 409–412.

ILLIAN, J., A. PENTTINEN, H. STOYAN and D. STOYAN (2008), *Statistical Analysis and Modelling of Spatial Point Patterns*, John Wiley & Sons, Chichester.

PARRENIN, F., G. DREYFUS, G. DURNAD, S. FUJITA, O. GAGLIARDINI, F. GILET, J. JOUZEL, K. KAWAMURA, N. LHOMME, V. MASSON-DELMOTTE, C. RITZ, J. SCHWANDER, H. SHOJI, R. UEMURA, O. WATANABE, and N. YOSHIDA (2007), 1-D-ice flow modelling at EPICA Dome C and Dome Fuji, East Antarctica, *Climate of the Past 3*, 243–259.

PATERSON, W. S. B. (1994), *The Physics of Glaciers*, Pergamon press, Oxford.

RUTH, U., J. BARNOLA, J. BEER, M. BIGLER, T. BLUNIER, E. CASTELLANO, H. FISCHER, F. FUNDEL, P. HUYBRECHTS, P. KAUFMANN, S. KIPFSTUHL, A. LAMBRECHT, A. MORGANTI, H. OERTER, F. PARRENIN, O. RYBAK, M. SEVERI, R. UDISTI, F. WILHELMS and E. WOLFF (2007), EDML1: A chronology for the EPICA deep ice core from Dronning Maud Land, Antarctica, over the last 150 000 years, *Climate of the Past 3*, 475–484.

SEVERI, M., S. BECAGLI, E. CASTELLANO, A. MORGANTI, R. TRAVERSI, R. UDISTI, U. RUTH, H. FISCHER, P. HUYBRECHTS, E. WOLFF, F. PAR-

RENIN, P. KAUFMANN, F. LAMBERT and J. P. STEFFENSEN (2007), Synchronisation of the EDML and EDC ice cores for the last 52 kyr by volcanic signature matching, *Climate of the Past 3*, 367–374.

STENNI, B., M. PROPOSITO, R. GRAGNANI, O. FLORA, J. JOUZEL, S. FALOURD and M. FREZOTTI (2002), Eight centuries of volcanic signal and climate change at Talos Dome (East Antartica), *Journal of Geophysical Research 107*(D9), 4076–4089.

STOYAN, D. (1991), Describing the anisotropy of marked planar point processes, *Statistics 22*, 449–462.

STOYAN, D. and V. BENEŠ (1991), Anisotropy analysis for particle systems, *Journal of microscopy 164*, 159–168.

STOYAN, D., W. S. KENDALL and J. MECKE (1995), *Stochastic Geometry and its Applications* (Second ed.), Wiley, Chichester.

STOYAN, D. and H. STOYAN (1994), *Fractals, Random Shapes and Point Fields*, John Wiley & Sons, Chichester.

Published reports of the Fraunhofer ITWM

The PDF-files of the following reports are available under:
www.itwm.fraunhofer.de/de/zentral__berichte/berichte

1. D. Hietel, K. Steiner, J. Struckmeier
A Finite - Volume Particle Method for Compressible Flows
(19 pages, 1998)

2. M. Feldmann, S. Seibold
Damage Diagnosis of Rotors: Application of Hilbert Transform and Multi-Hypothesis Testing
Keywords: Hilbert transform, damage diagnosis, Kalman filtering, non-linear dynamics
(23 pages, 1998)

3. Y. Ben-Haim, S. Seibold
Robust Reliability of Diagnostic Multi-Hypothesis Algorithms: Application to Rotating Machinery
Keywords: Robust reliability, convex models, Kalman filtering, multi-hypothesis diagnosis, rotating machinery, crack diagnosis
(24 pages, 1998)

4. F.-Th. Lentes, N. Siedow
Three-dimensional Radiative Heat Transfer in Glass Cooling Processes
(23 pages, 1998)

5. A. Klar, R. Wegener
A hierarchy of models for multilane vehicular traffic
Part I: Modeling
(23 pages, 1998)

Part II: Numerical and stochastic investigations
(17 pages, 1998)

6. A. Klar, N. Siedow
Boundary Layers and Domain Decomposition for Radiative Heat Transfer and Diffusion Equations: Applications to Glass Manufacturing Processes
(24 pages, 1998)

7. I. Choquet
Heterogeneous catalysis modelling and numerical simulation in rarified gas flows Part I: Coverage locally at equilibrium
(24 pages, 1998)

8. J. Ohser, B. Steinbach, C. Lang
Efficient Texture Analysis of Binary Images
(17 pages, 1998)

9. J. Orlik
Homogenization for viscoelasticity of the integral type with aging and shrinkage
(20 pages, 1998)

10. J. Mohring
Helmholtz Resonators with Large Aperture
(21 pages, 1998)

11. H. W. Hamacher, A. Schöbel
On Center Cycles in Grid Graphs
(15 pages, 1998)

12. H. W. Hamacher, K.-H. Küfer
Inverse radiation therapy planning - a multiple objective optimisation approach
(14 pages, 1999)

13. C. Lang, J. Ohser, R. Hilfer
On the Analysis of Spatial Binary Images
(20 pages, 1999)

14. M. Junk
On the Construction of Discrete Equilibrium Distributions for Kinetic Schemes
(24 pages, 1999)

15. M. Junk, S. V. Raghurame Rao
A new discrete velocity method for Navier-Stokes equations
(20 pages, 1999)

16. H. Neunzert
Mathematics as a Key to Key Technologies
(39 pages (4 PDF-Files), 1999)

17. J. Ohser, K. Sandau
Considerations about the Estimation of the Size Distribution in Wicksell's Corpuscle Problem
(18 pages, 1999)

18. E. Carrizosa, H. W. Hamacher, R. Klein, S. Nickel
Solving nonconvex planar location problems by finite dominating sets
Keywords: Continuous Location, Polyhedral Gauges, Finite Dominating Sets, Approximation, Sandwich Algorithm, Greedy Algorithm
(19 pages, 2000)

19. A. Becker
A Review on Image Distortion Measures
Keywords: Distortion measure, human visual system
(26 pages, 2000)

20. H. W. Hamacher, M. Labbé, S. Nickel, T. Sonneborn
Polyhedral Properties of the Uncapacitated Multiple Allocation Hub Location Problem
Keywords: integer programming, hub location, facility location, valid inequalities, facets, branch and cut
(21 pages, 2000)

21. H. W. Hamacher, A. Schöbel
Design of Zone Tariff Systems in Public Transportation
(30 pages, 2001)

22. D. Hietel, M. Junk, R. Keck, D. Teleaga
The Finite-Volume-Particle Method for Conservation Laws
(16 pages, 2001)

23. T. Bender, H. Hennes, J. Kalcsics, M. T. Melo, S. Nickel
Location Software and Interface with GIS and Supply Chain Management
Keywords: facility location, software development, geographical information systems, supply chain management
(48 pages, 2001)

24. H. W. Hamacher, S. A. Tjandra
Mathematical Modelling of Evacuation Problems: A State of Art
(44 pages, 2001)

25. J. Kuhnert, S. Tiwari
Grid free method for solving the Poisson equation
Keywords: Poisson equation, Least squares method, Grid free method
(19 pages, 2001)

26. T. Götz, H. Rave, D. Reinel-Bitzer, K. Steiner, H. Tiemeier
Simulation of the fiber spinning process
Keywords: Melt spinning, fiber model, Lattice Boltzmann, CFD
(19 pages, 2001)

27. A. Zemitis
On interaction of a liquid film with an obstacle
Keywords: impinging jets, liquid film, models, numerical solution, shape
(22 pages, 2001)

28. I. Ginzburg, K. Steiner
Free surface lattice-Boltzmann method to model the filling of expanding cavities by Bingham Fluids
Keywords: Generalized LBE, free-surface phenomena, interface boundary conditions, filling processes, Bingham viscoplastic model, regularized models
(22 pages, 2001)

29. H. Neunzert
»Denn nichts ist für den Menschen als Menschen etwas wert, was er nicht mit Leidenschaft tun kann«
Vortrag anlässlich der Verleihung des Akademiepreises des Landes Rheinland-Pfalz am 21.11.2001
Keywords: Lehre, Forschung, angewandte Mathematik, Mehrskalenanalyse, Strömungsmechanik
(18 pages, 2001)

30. J. Kuhnert, S. Tiwari
Finite pointset method based on the projection method for simulations of the incompressible Navier-Stokes equations
Keywords: Incompressible Navier-Stokes equations, Meshfree method, Projection method, Particle scheme, Least squares approximation
AMS subject classification: 76D05, 76M28
(25 pages, 2001)

31. R. Korn, M. Krekel
Optimal Portfolios with Fixed Consumption or Income Streams
Keywords: Portfolio optimisation, stochastic control, HJB equation, discretisation of control problems
(23 pages, 2002)

32. M. Krekel
Optimal portfolios with a loan dependent credit spread
Keywords: Portfolio optimisation, stochastic control, HJB equation, credit spread, log utility, power utility, non-linear wealth dynamics
(25 pages, 2002)

33. J. Ohser, W. Nagel, K. Schladitz
The Euler number of discretized sets – on the choice of adjacency in homogeneous lattices
Keywords: image analysis, Euler number, neighborhod relationships, cuboidal lattice
(32 pages, 2002)

34. I. Ginzburg, K. Steiner
Lattice Boltzmann Model for Free-Surface flow and Its Application to Filling Process in Casting
Keywords: Lattice Boltzmann models; free-surface phenomena; interface boundary conditions; filling processes; injection molding; volume of fluid method; interface boundary conditions; advection-schemes; upwind-schemes
(54 pages, 2002)

35. M. Günther, A. Klar, T. Materne, R. Wegener
Multivalued fundamental diagrams and stop and go waves for continuum traffic equations
Keywords: traffic flow, macroscopic equations, kinetic derivation, multivalued fundamental diagram, stop and go waves, phase transitions
(25 pages, 2002)

36. S. Feldmann, P. Lang, D. Prätzel-Wolters
Parameter influence on the zeros of network determinants
Keywords: Networks, Equicofactor matrix polynomials, Realization theory, Matrix perturbation theory
(30 pages, 2002)

37. K. Koch, J. Ohser, K. Schladitz
Spectral theory for random closed sets and estimating the covariance via frequency space
Keywords: Random set, Bartlett spectrum, fast Fourier transform, power spectrum
(28 pages, 2002)

38. D. d'Humières, I. Ginzburg
Multi-reflection boundary conditions for lattice Boltzmann models
Keywords: lattice Boltzmann equation, boudary condistions, bounce-back rule, Navier-Stokes equation
(72 pages, 2002)

39. R. Korn
Elementare Finanzmathematik
Keywords: Finanzmathematik, Aktien, Optionen, Portfolio-Optimierung, Börse, Lehrerweiterbildung, Mathematikunterricht
(98 pages, 2002)

40. J. Kallrath, M. C. Müller, S. Nickel
Batch Presorting Problems: Models and Complexity Results
Keywords: Complexity theory, Integer programming, Assigment, Logistics
(19 pages, 2002)

41. J. Linn
On the frame-invariant description of the phase space of the Folgar-Tucker equation
Key words: fiber orientation, Folgar-Tucker equation, injection molding
(5 pages, 2003)

42. T. Hanne, S. Nickel
A Multi-Objective Evolutionary Algorithm for Scheduling and Inspection Planning in Software Development Projects
Key words: multiple objective programming, project management and scheduling, software development, evolutionary algorithms, efficient set
(29 pages, 2003)

43. T. Bortfeld , K.-H. Küfer, M. Monz, A. Scherrer, C. Thieke, H. Trinkaus
Intensity-Modulated Radiotherapy - A Large Scale Multi-Criteria Programming Problem
Keywords: multiple criteria optimization, representative systems of Pareto solutions, adaptive triangulation, clustering and disaggregation techniques, visualization of Pareto solutions, medical physics, external beam radiotherapy planning, intensity modulated radiotherapy
(31 pages, 2003)

44. T. Halfmann, T. Wichmann
Overview of Symbolic Methods in Industrial Analog Circuit Design
Keywords: CAD, automated analog circuit design, symbolic analysis, computer algebra, behavioral modeling, system simulation, circuit sizing, macro modeling, differential-algebraic equations, index
(17 pages, 2003)

45. S. E. Mikhailov, J. Orlik
Asymptotic Homogenisation in Strength and Fatigue Durability Analysis of Composites
Keywords: multiscale structures, asymptotic homogenization, strength, fatigue, singularity, non-local conditions
(14 pages, 2003)

46. P. Domínguez-Marín, P. Hansen, N. Mladenovi´c , S. Nickel
Heuristic Procedures for Solving the Discrete Ordered Median Problem
Keywords: genetic algorithms, variable neighborhood search, discrete facility location
(31 pages, 2003)

47. N. Boland, P. Domínguez-Marín, S. Nickel, J. Puerto
Exact Procedures for Solving the Discrete Ordered Median Problem
Keywords: discrete location, Integer programming
(41 pages, 2003)

48. S. Feldmann, P. Lang
Padé-like reduction of stable discrete linear systems preserving their stability
Keywords: Discrete linear systems, model reduction, stability, Hankel matrix, Stein equation
(16 pages, 2003)

49. J. Kallrath, S. Nickel
A Polynomial Case of the Batch Presorting Problem
Keywords: batch presorting problem, online optimization, competetive analysis, polynomial algorithms, logistics
(17 pages, 2003)

50. T. Hanne, H. L. Trinkaus
knowCube for MCDM – Visual and Interactive Support for Multicriteria Decision Making
Key words: Multicriteria decision making, knowledge management, decision support systems, visual interfaces, interactive navigation, real-life applications.
(26 pages, 2003)

51. O. Iliev, V. Laptev
On Numerical Simulation of Flow Through Oil Filters
Keywords: oil filters, coupled flow in plain and porous media, Navier-Stokes, Brinkman, numerical simulation
(8 pages, 2003)

52. W. Dörfler, O. Iliev, D. Stoyanov, D. Vassileva
On a Multigrid Adaptive Refinement Solver for Saturated Non-Newtonian Flow in Porous Media
Keywords: Nonlinear multigrid, adaptive refinement, non-Newtonian flow in porous media
(17 pages, 2003)

53. S. Kruse
On the Pricing of Forward Starting Options under Stochastic Volatility
Keywords: Option pricing, forward starting options, Heston model, stochastic volatility, cliquet options
(11 pages, 2003)

54. O. Iliev, D. Stoyanov
Multigrid – adaptive local refinement solver for incompressible flows
Keywords: Navier-Stokes equations, incompressible flow, projection-type splitting, SIMPLE, multigrid methods, adaptive local refinement, lid-driven flow in a cavity
(37 pages, 2003)

55. V. Starikovicius
The multiphase flow and heat transfer in porous media
Keywords: Two-phase flow in porous media, various formulations, global pressure, multiphase mixture model, numerical simulation
(30 pages, 2003)

56. P. Lang, A. Sarishvili, A. Wirsen
Blocked neural networks for knowledge extraction in the software development process
Keywords: Blocked Neural Networks, Nonlinear Regression, Knowledge Extraction, Code Inspection
(21 pages, 2003)

57. H. Knaf, P. Lang, S. Zeiser
Diagnosis aiding in Regulation Thermography using Fuzzy Logic
Keywords: fuzzy logic,knowledge representation, expert system
(22 pages, 2003)

58. M. T. Melo, S. Nickel, F. Saldanha da Gama
Largescale models for dynamic multicommodity capacitated facility location
Keywords: supply chain management, strategic planning, dynamic location, modeling
(40 pages, 2003)

59. J. Orlik
Homogenization for contact problems with periodically rough surfaces
Keywords: asymptotic homogenization, contact problems
(28 pages, 2004)

60. A. Scherrer, K.-H. Küfer, M. Monz, F. Alonso, T. Bortfeld
IMRT planning on adaptive volume structures – a significant advance of computational complexity
Keywords: Intensity-modulated radiation therapy (IMRT), inverse treatment planning, adaptive volume structures, hierarchical clustering, local refinement, adaptive clustering, convex programming, mesh generation, multi-grid methods
(24 pages, 2004)

61. D. Kehrwald
Parallel lattice Boltzmann simulation of complex flows
Keywords: Lattice Boltzmann methods, parallel computing, microstructure simulation, virtual material design, pseudo-plastic fluids, liquid composite moulding
(12 pages, 2004)

62. O. Iliev, J. Linn, M. Moog, D. Niedziela, V. Starikovicius
On the Performance of Certain Iterative Solvers for Coupled Systems Arising in Discretization of Non-Newtonian Flow Equations
Keywords: Performance of iterative solvers, Preconditioners, Non-Newtonian flow
(17 pages, 2004)

63. R. Ciegis, O. Iliev, S. Rief, K. Steiner
On Modelling and Simulation of Different Regimes for Liquid Polymer Moulding
Keywords: Liquid Polymer Moulding, Modelling, Simulation, Infiltration, Front Propagation, non-Newtonian flow in porous media
(43 pages, 2004)

64. T. Hanne, H. Neu
Simulating Human Resources in Software Development Processes
Keywords: Human resource modeling, software process, productivity, human factors, learning curve
(14 pages, 2004)

65. O. Iliev, A. Mikelic, P. Popov
Fluid structure interaction problems in deformable porous media: Toward permeability of deformable porous media
Keywords: fluid-structure interaction, deformable porous media, upscaling, linear elasticity, stokes, finite elements
(28 pages, 2004)

66. F. Gaspar, O. Iliev, F. Lisbona, A. Naumovich, P. Vabishchevich
On numerical solution of 1-D poroelasticity equations in a multilayered domain
Keywords: poroelasticity, multilayered material, finite volume discretization, MAC type grid
(41 pages, 2004)

67. J. Ohser, K. Schladitz, K. Koch, M. Nöthe
Diffraction by image processing and its application in materials science
Keywords: porous microstructure, image analysis, random set, fast Fourier transform, power spectrum, Bartlett spectrum
(13 pages, 2004)

68. H. Neunzert
Mathematics as a Technology: Challenges for the next 10 Years
Keywords: applied mathematics, technology, modelling, simulation, visualization, optimization, glass processing, spinning processes, fiber-fluid interaction, trubulence effects, topological optimization, multicriteria optimization, Uncertainty and Risk, financial mathematics, Malliavin calculus, Monte-Carlo methods, virtual material design, filtration, bio-informatics, system biology
(29 pages, 2004)

69. R. Ewing, O. Iliev, R. Lazarov, A. Naumovich
On convergence of certain finite difference discretizations for 1D poroelasticity interface problems
Keywords: poroelasticity, multilayered material, finite volume discretizations, MAC type grid, error estimates
(26 pages,2004)

70. W. Dörfler, O. Iliev, D. Stoyanov, D. Vassileva
On Efficient Simulation of Non-Newtonian Flow in Saturated Porous Media with a Multigrid Adaptive Refinement Solver
Keywords: Nonlinear multigrid, adaptive renement, non-Newtonian in porous media
(25 pages, 2004)

71. J. Kalcsics, S. Nickel, M. Schröder
Towards a Unified Territory Design Approach – Applications, Algorithms and GIS Integration
Keywords: territory desgin, political districting, sales territory alignment, optimization algorithms, Geographical Information Systems
(40 pages, 2005)

72. K. Schladitz, S. Peters, D. Reinel-Bitzer, A. Wiegmann, J. Ohser
Design of acoustic trim based on geometric modeling and flow simulation for non-woven
Keywords: random system of fibers, Poisson line process, flow resistivity, acoustic absorption, Lattice-Boltzmann method, non-woven
(21 pages, 2005)

73. V. Rutka, A. Wiegmann
Explicit Jump Immersed Interface Method for virtual material design of the effective elastic moduli of composite materials
Keywords: virtual material design, explicit jump immersed interface method, effective elastic moduli, composite materials
(22 pages, 2005)

74. T. Hanne
Eine Übersicht zum Scheduling von Baustellen
Keywords: Projektplanung, Scheduling, Bauplanung, Bauindustrie
(32 pages, 2005)

75. J. Linn
The Folgar-Tucker Model as a Differetial Algebraic System for Fiber Orientation Calculation
Keywords: fiber orientation, Folgar–Tucker model, invariants, algebraic constraints, phase space, trace stability
(15 pages, 2005)

76. M. Speckert, K. Dreßler, H. Mauch, A. Lion, G. J. Wierda
Simulation eines neuartigen Prüfsystems für Achserprobungen durch MKS-Modellierung einschließlich Regelung
Keywords: virtual test rig, suspension testing, multibody simulation, modeling hexapod test rig, optimization of test rig configuration
(20 pages, 2005)

77. K.-H. Küfer, M. Monz, A. Scherrer, P. Süss, F. Alonso, A. S. A. Sultan, Th. Bortfeld, D. Craft, Chr. Thieke
Multicriteria optimization in intensity modulated radiotherapy planning
Keywords: multicriteria optimization, extreme solutions, real-time decision making, adaptive approximation schemes, clustering methods, IMRT planning, reverse engineering
(51 pages, 2005)

78. S. Amstutz, H. Andrä
A new algorithm for topology optimization using a level-set method
Keywords: shape optimization, topology optimization, topological sensitivity, level-set
(22 pages, 2005)

79. N. Ettrich
Generation of surface elevation models for urban drainage simulation
Keywords: Flooding, simulation, urban elevation models, laser scanning
(22 pages, 2005)

80. H. Andrä, J. Linn, I. Matei, I. Shklyar, K. Steiner, E. Teichmann
OPTCAST – Entwicklung adäquater Strukturoptimierungsverfahren für Gießereien Technischer Bericht (KURZFASSUNG)
Keywords: Topologieoptimierung, Level-Set-Methode, Gießprozesssimulation, Gießtechnische Restriktionen, CAE-Kette zur Strukturoptimierung
(77 pages, 2005)

81. N. Marheineke, R. Wegener
Fiber Dynamics in Turbulent Flows Part I: General Modeling Framework
Keywords: fiber-fluid interaction; Cosserat rod; turbulence modeling; Kolmogorov's energy spectrum; double-velocity correlations; differentiable Gaussian fields
(20 pages, 2005)

Part II: Specific Taylor Drag
Keywords: flexible fibers; k-ε turbulence model; fiber-turbulence interaction scales; air drag; random Gaussian aerodynamic force; white noise; stochastic differential equations; ARMA process
(18 pages, 2005)

82. C. H. Lampert, O. Wirjadi
An Optimal Non-Orthogonal Separation of the Anisotropic Gaussian Convolution Filter
Keywords: Anisotropic Gaussian filter, linear filtering, orientation space, nD image processing, separable filters
(25 pages, 2005)

83. H. Andrä, D. Stoyanov
Error indicators in the parallel finite element solver for linear elasticity DDFEM
Keywords: linear elasticity, finite element method, hierarchical shape functions, domain decom-position, parallel implementation, a posteriori error estimates
(21 pages, 2006)

84. M. Schröder, I. Solchenbach
Optimization of Transfer Quality in Regional Public Transit
Keywords: public transit, transfer quality, quadratic assignment problem
(16 pages, 2006)

85. A. Naumovich, F. J. Gaspar
On a multigrid solver for the three-dimensional Biot poroelasticity system in multilayered domains
Keywords: poroelasticity, interface problem, multigrid, operator-dependent prolongation
(11 pages, 2006)

86. S. Panda, R. Wegener, N. Marheineke
Slender Body Theory for the Dynamics of Curved Viscous Fibers
Keywords: curved viscous fibers; fluid dynamics; Navier-Stokes equations; free boundary value problem; asymptotic expansions; slender body theory
(14 pages, 2006)

87. E. Ivanov, H. Andrä, A. Kudryavtsev
Domain Decomposition Approach for Automatic Parallel Generation of Tetrahedral Grids
Key words: Grid Generation, Unstructured Grid, Delaunay Triangulation, Parallel Programming, Domain Decomposition, Load Balancing
(18 pages, 2006)

88. S. Tiwari, S. Antonov, D. Hietel, J. Kuhnert, R. Wegener
A Meshfree Method for Simulations of Interactions between Fluids and Flexible Structures
Key words: Meshfree Method, FPM, Fluid Structure Interaction, Sheet of Paper, Dynamical Coupling
(16 pages, 2006)

89. R. Ciegis , O. Iliev, V. Starikovicius, K. Steiner
Numerical Algorithms for Solving Problems of Multiphase Flows in Porous Media
Keywords: nonlinear algorithms, finite-volume method, software tools, porous media, flows
(16 pages, 2006)

90. D. Niedziela, O. Iliev, A. Latz
On 3D Numerical Simulations of Viscoelastic Fluids
Keywords: non-Newtonian fluids, anisotropic viscosity, integral constitutive equation
(18 pages, 2006)

91. A. Winterfeld
Application of general semi-infinite Programming to Lapidary Cutting Problems
Keywords: large scale optimization, nonlinear programming, general semi-infinite optimization, design centering, clustering
(26 pages, 2006)

92. J. Orlik, A. Ostrovska
Space-Time Finite Element Approximation and Numerical Solution of Hereditary Linear Viscoelasticity Problems
Keywords: hereditary viscoelasticity; kern approximation by interpolation; space-time finite element approximation, stability and a priori estimate
(24 pages, 2006)

93. V. Rutka, A. Wiegmann, H. Andrä
EJIIM for Calculation of effective Elastic Moduli in 3D Linear Elasticity
Keywords: Elliptic PDE, linear elasticity, irregular domain, finite differences, fast solvers, effective elastic moduli
(24 pages, 2006)

94. A. Wiegmann, A. Zemitis
EJ-HEAT: A Fast Explicit Jump Harmonic Averaging Solver for the Effective Heat Conductivity of Composite Materials
Keywords: Stationary heat equation, effective thermal conductivity, explicit jump, discontinuous coefficients, virtual material design, microstructure simulation, EJ-HEAT
(21 pages, 2006)

95. A. Naumovich
On a finite volume discretization of the three-dimensional Biot poroelasticity system in multilayered domains
Keywords: Biot poroelasticity system, interface problems, finite volume discretization, finite difference method
(21 pages, 2006)

96. M. Krekel, J. Wenzel
A unified approach to Credit Default Swaption and Constant Maturity Credit Default Swap valuation
Keywords: LIBOR market model, credit risk, Credit Default Swaption, Constant Maturity Credit Default Swap-method
(43 pages, 2006)

97. A. Dreyer
Interval Methods for Analog Circiuts
Keywords: interval arithmetic, analog circuits, tolerance analysis, parametric linear systems, frequency response, symbolic analysis, CAD, computer algebra
(36 pages, 2006)

98. N. Weigel, S. Weihe, G. Bitsch, K. Dreßler
Usage of Simulation for Design and Optimization of Testing
Keywords: Vehicle test rigs, MBS, control, hydraulics, testing philosophy
(14 pages, 2006)

99. H. Lang, G. Bitsch, K. Dreßler, M. Speckert
Comparison of the solutions of the elastic and elastoplastic boundary value problems
Keywords: Elastic BVP, elastoplastic BVP, variational inequalities, rate-independency, hysteresis, linear kinematic hardening, stop- and play-operator
(21 pages, 2006)

100. M. Speckert, K. Dreßler, H. Mauch
MBS Simulation of a hexapod based suspension test rig
Keywords: Test rig, MBS simulation, suspension, hydraulics, controlling, design optimization
(12 pages, 2006)

101. S. Azizi Sultan, K.-H. Küfer
A dynamic algorithm for beam orientations in multicriteria IMRT planning
Keywords: radiotherapy planning, beam orientation optimization, dynamic approach, evolutionary algorithm, global optimization
(14 pages, 2006)

102. T. Götz, A. Klar, N. Marheineke, R. Wegener
A Stochastic Model for the Fiber Lay-down Process in the Nonwoven Production
Keywords: fiber dynamics, stochastic Hamiltonian system, stochastic averaging
(17 pages, 2006)

103. Ph. Süss, K.-H. Küfer
Balancing control and simplicity: a variable aggregation method in intensity modulated radiation therapy planning
Keywords: IMRT planning, variable aggregation, clustering methods
(22 pages, 2006)

104. A. Beaudry, G. Laporte, T. Melo, S. Nickel
Dynamic transportation of patients in hospitals
Keywords: in-house hospital transportation, dial-a-ride, dynamic mode, tabu search
(37 pages, 2006)

105. Th. Hanne
Applying multiobjective evolutionary algorithms in industrial projects
Keywords: multiobjective evolutionary algorithms, discrete optimization, continuous optimization, electronic circuit design, semi-infinite programming, scheduling
(18 pages, 2006)

106. J. Franke, S. Halim
Wild bootstrap tests for comparing signals and images
Keywords: wild bootstrap test, texture classification, textile quality control, defect detection, kernel estimate, nonparametric regression
(13 pages, 2007)

107. Z. Drezner, S. Nickel
Solving the ordered one-median problem in the plane
Keywords: planar location, global optimization, ordered median, big triangle small triangle method, bounds, numerical experiments
(21 pages, 2007)

108. Th. Götz, A. Klar, A. Unterreiter, R. Wegener
Numerical evidance for the non-existing of solutions of the equations desribing rotational fiber spinning
Keywords: rotational fiber spinning, viscous fibers, boundary value problem, existence of solutions
(11 pages, 2007)

109. Ph. Süss, K.-H. Küfer
Smooth intensity maps and the Bortfeld-Boyer sequencer
Keywords: probabilistic analysis, intensity modulated radiotherapy treatment (IMRT), IMRT plan application, step-and-shoot sequencing
(8 pages, 2007)

110. E. Ivanov, O. Gluchshenko, H. Andrä, A. Kudryavtsev
Parallel software tool for decomposing and meshing of 3d structures
Keywords: a-priori domain decomposition, unstructured grid, Delaunay mesh generation
(14 pages, 2007)

111. O. Iliev, R. Lazarov, J. Willems
Numerical study of two-grid preconditioners for 1d elliptic problems with highly oscillating discontinuous coefficients
Keywords: two-grid algorithm, oscillating coefficients, preconditioner
(20 pages, 2007)

112. L. Bonilla, T. Götz, A. Klar, N. Marheineke, R. Wegener
Hydrodynamic limit of the Fokker-Planck-equation describing fiber lay-down processes
Keywords: stochastic dierential equations, Fokker-Planck equation, asymptotic expansion, Ornstein-Uhlenbeck process
(17 pages, 2007)

113. S. Rief
Modeling and simulation of the pressing section of a paper machine
Keywords: paper machine, computational fluid dynamics, porous media
(41 pages, 2007)

114. R. Ciegis, O. Iliev, Z. Lakdawala
On parallel numerical algorithms for simulating industrial filtration problems
Keywords: Navier-Stokes-Brinkmann equations, finite volume discretization method, SIMPLE, parallel computing, data decomposition method
(24 pages, 2007)

115. N. Marheineke, R. Wegener
Dynamics of curved viscous fibers with surface tension
Keywords: Slender body theory, curved viscous bers with surface tension, free boundary value problem
(25 pages, 2007)

116. S. Feth, J. Franke, M. Speckert
Resampling-Methoden zur mse-Korrektur und Anwendungen in der Betriebsfestigkeit
Keywords: Weibull, Bootstrap, Maximum-Likelihood, Betriebsfestigkeit
(16 pages, 2007)

117. H. Knaf
Kernel Fisher discriminant functions – a concise and rigorous introduction
Keywords: wild bootstrap test, texture classification, textile quality control, defect detection, kernel estimate, nonparametric regression
(30 pages, 2007)

118. O. Iliev, I. Rybak
On numerical upscaling for flows in heterogeneous porous media
Keywords: numerical upscaling, heterogeneous porous media, single phase flow, Darcy's law, multiscale problem, effective permeability, multipoint flux approximation, anisotropy
(17 pages, 2007)

119. O. Iliev, I. Rybak
On approximation property of multipoint flux approximation method
Keywords: Multipoint flux approximation, finite volume method, elliptic equation, discontinuous tensor coefficients, anisotropy
(15 pages, 2007)

120. O. Iliev, I. Rybak, J. Willems
On upscaling heat conductivity for a class of industrial problems
Keywords: Multiscale problems, effective heat conductivity, numerical upscaling, domain decomposition
(21 pages, 2007)

121. R. Ewing, O. Iliev, R. Lazarov, I. Rybak
On two-level preconditioners for flow in porous media
Keywords: Multiscale problem, Darcy's law, single phase flow, anisotropic heterogeneous porous media, numerical upscaling, multigrid, domain decomposition, efficient preconditioner
(18 pages, 2007)

122. M. Brickenstein, A. Dreyer
POLYBORI: A Gröbner basis framework for Boolean polynomials
Keywords: Gröbner basis, formal verification, Boolean polynomials, algebraic cryptoanalysis, satisfiability
(23 pages, 2007)

123. O. Wirjadi
Survey of 3d image segmentation methods
Keywords: image processing, 3d, image segmentation, binarization
(20 pages, 2007)

124. S. Zeytun, A. Gupta
A Comparative Study of the Vasicek and the CIR Model of the Short Rate
Keywords: interest rates, Vasicek model, CIR-model, calibration, parameter estimation
(17 pages, 2007)

125. G. Hanselmann, A. Sarishvili
Heterogeneous redundancy in software quality prediction using a hybrid Bayesian approach
Keywords: reliability prediction, fault prediction, non-homogeneous poisson process, Bayesian model averaging
(17 pages, 2007)

126. V. Maag, M. Berger, A. Winterfeld, K.-H. Küfer
A novel non-linear approach to minimal area rectangular packing
Keywords: rectangular packing, non-overlapping constraints, non-linear optimization, regularization, relaxation
(18 pages, 2007)

127. M. Monz, K.-H. Küfer, T. Bortfeld, C. Thieke
Pareto navigation – systematic multi-criteria-based IMRT treatment plan determination
Keywords: convex, interactive multi-objective optimization, intensity modulated radiotherapy planning
(15 pages, 2007)

128. M. Krause, A. Scherrer
On the role of modeling parameters in IMRT plan optimization
Keywords: intensity-modulated radiotherapy (IMRT), inverse IMRT planning, convex optimization, sensitivity analysis, elasticity, modeling parameters, equivalent uniform dose (EUD)
(18 pages, 2007)

129. A. Wiegmann
Computation of the permeability of porous materials from their microstructure by FFF-Stokes
Keywords: permeability, numerical homogenization, fast Stokes solver
(24 pages, 2007)

130. T. Melo, S. Nickel, F. Saldanha da Gama
Facility Location and Supply Chain Management – A comprehensive review
Keywords: facility location, supply chain management, network design
(54 pages, 2007)

131. T. Hanne, T. Melo, S. Nickel
Bringing robustness to patient flow management through optimized patient transports in hospitals
Keywords: Dial-a-Ride problem, online problem, case study, tabu search, hospital logistics
(23 pages, 2007)

132. R. Ewing, O. Iliev, R. Lazarov, I. Rybak, J. Willems
An efficient approach for upscaling properties of composite materials with high contrast of coefficients
Keywords: effective heat conductivity, permeability of fractured porous media, numerical upscaling, fibrous insulation materials, metal foams
(16 pages, 2008)

133. S. Gelareh, S. Nickel
New approaches to hub location problems in public transport planning
Keywords: integer programming, hub location, transportation, decomposition, heuristic
(25 pages, 2008)

134. G. Thömmes, J. Becker, M. Junk, A. K. Vaikuntam, D. Kehrwald, A. Klar, K. Steiner, A. Wiegmann
A Lattice Boltzmann Method for immiscible multiphase flow simulations using the Level Set Method
Keywords: Lattice Boltzmann method, Level Set method, free surface, multiphase flow
(28 pages, 2008)

135. J. Orlik
Homogenization in elasto-plasticity
Keywords: multiscale structures, asymptotic homogenization, nonlinear energy
(40 pages, 2008)

136. J. Almquist, H. Schmidt, P. Lang, J. Deitmer, M. Jirstrand, D. Prätzel-Wolters, H. Becker
Determination of interaction between MCT1 and CAII via a mathematical and physiological approach
Keywords: mathematical modeling; model reduction; electrophysiology; pH-sensitive microelectrodes; proton antenna
(20 pages, 2008)

137. E. Savenkov, H. Andrä, O. Iliev
An analysis of one regularization approach for solution of pure Neumann problem
Keywords: pure Neumann problem, elasticity, regularization, finite element method, condition number
(27 pages, 2008)

138. O. Berman, J. Kalcsics, D. Krass, S. Nickel
The ordered gradual covering location problem on a network
Keywords: gradual covering, ordered median function, network location
(32 pages, 2008)

139. S. Gelareh, S. Nickel
Multi-period public transport design: A novel model and solution approaches
Keywords: Integer programming, hub location, public transport, multi-period planning, heuristics
(31 pages, 2008)

140. T. Melo, S. Nickel, F. Saldanha-da-Gama
Network design decisions in supply chain planning
Keywords: supply chain design, integer programming models, location models, heuristics
(20 pages, 2008)

141. C. Lautensack, A. Särkkä, J. Freitag, K. Schladitz
Anisotropy analysis of pressed point processes
Keywords: estimation of compression, isotropy test, nearest neighbour distance, orientation analysis, polar ice, Ripley's K function
(35 pages, 2008)

Status quo: June 2008